HUITE BOOTSMA

GROUNDWATER RECHARGE ON THE CULTUURVLAKTE OF ST. EUSTATIUS

GROUNDWATER RECHARGE ON THE CULTUURVLAKTE OF ST. EUSTATIUS

HUITE BOOTSMA

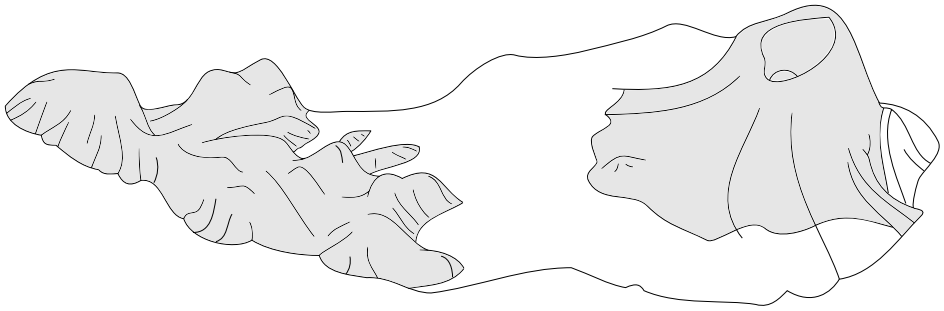

MSc Thesis

Soil Physics and Land Management Group
Wageningen University

June 2015

Huite Bootsma: *Groundwater Recharge on the Cultuurvlakte of St. Eustatius* , June 2015

SUPERVISORS:
Klaas Metselaar
Jos van Dam

LOCATION:
Wageningen

ABSTRACT

Groundwater is an important resource and an important factor to consider in pollution management. Accurate estimates of groundwater recharge are essential for effective management of groundwater. St. Eustatius is a small island of the Leeward Islands in the Caribbean Sea with a brackish groundwater lens with high nutrient concentrations at the inhabitated part of the island. In this study, groundwater recharge was estimated with a modelling approach, using the unsaturated zone model SWAP. A period of 30 years was simulated. Field work was performed on St. Eustatius to determine vegetation and soil parameters.

Model calculations show that for the inhabited part of the island, the Cultuurvlakte, long term average groundwater recharge ranges 75–210 mm $year^{-1}$. Quantitative uncertainty bounds could not be determined. High groundwater nitrogen concentrations suggest that in some parts of the Cultuurvlakte a third to all of groundwater is infiltrated sewage water.

A global sensitivity analysis was performed using the Morris method. The sensitivity analysis showed that rainfall is the most important factor in determining groundwater recharge, followed by reference evapotranspiration and vegetation characteristics that control evapotranspirative fluxes. Rainfall intensity and antecedent soil moisture play a key role in generating groundwater recharge; a simple conceptual reservoir model proved capable of reproducing the recharge simulated by SWAP. The results emphasize the importance of accurate rainfall measurements and the need to develop methods for estimating the evapotranspiration of natural vegetation.

ACKNOWLEDGMENTS

I thank my supervisors Klaas Metselaar and Jos van Dam, ever encouraging and accessible. On St. Eustatius, I thank the people at the LVV, who were always willing to assist in practical affairs. I am also especially grateful towards George and Shelley Works, who provided me with crucial meteorological data: this research would have been much harder without. Finally, I thank my fellow students and friends, Wouter ten Harkel, Joeri van Engelen, and Walter Box: Wouter for company and assistance on St. Eustatius, and Joeri and Walter for hearing out my puzzlements and considerations.

CONTENTS

LIST OF FIGURES

LIST OF TABLES

LIST OF SYMBOLS

In order of appearance:

SYMBOL	UNITS	DESCRIPTION
θ	$cm^3\ cm^{-3}$	Volumetric moisture content
t	d	Time
K	$cm\ d^{-1}$	Hydraulic conductivity
h	cm	Soil water pressure head
z	cm	Height
S_a	$cm^3\ cm^{-3}\ d^{-1}$	Plant root water uptake
R_s	$MJ\ m^{-2}\ d^{-1}$	Daily solar shortwave radiation
R_a	$MJ\ m^{-2}\ d^{-1}$	Daily extraterrestrial radiation
K_{Rs}	$°C^{-0.5}$	Hargreaves radiation coefficient
ΔT	°C	Diurnal temperature range
T_{max}	°C	Maximum daily temperature
T_{min}	°C	Minimum daily temperature
RH	-	Relative humidity
τ_{max}	-	Maximum shortwave radiation transmittance
C_1	$°C^{-C_2}$	Campbell-Bristow coefficient

C_2	-	Campbell-Bristow coefficient
K_1	-	Modified-Hargreaves coefficient
K_2	-	Modified-Hargreaves coefficient
K_3	MJ m^{-2} d^{-1}	Modified-Hargreaves coefficient
ET_{ref}	mm d^{-1}	Reference evapotranspiration
Δ_v	kPa $°C^{-1}$	Vapour curve slope
R_n	MJ m^{-2} d^{-1}	Net solar radiation
G	MJ m^{-2} d^{-1}	Soil heat flux
γ	kPa $°C^{-1}$	Psychometric constant
u_2	m s^{-1}	Wind speed at 2 m height
e_s	kPa	Saturation vapour pressure
e_a	kPa	Actual vapour pressure
D50	m	Depth above which 50% of roots are located
D95	m	Depth above which 95% of roots are located
r_d	-	Root density
c_r	-	Root distribution shape parameter
D^*	-	Relative rooting depth
D	m	Depth below surface
θ_s	cm^3 cm^{-3}	Saturated water content
θ_r	cm^3 cm^{-3}	Residual water content
α	cm^{-1}	Van Genuchten-Mualem shape factor
m	-	Van Genuchten-Mualem shape factor
n	-	Van Genuchten-Mualem shape factor
λ	-	Van Genuchten-Mualem shape factor
K_s	cm d^{-1}	Saturated hydraulic conductivity
S_e	-	Relative water saturation
Cl	%	Mass percentage clay
Sa	%	Mass percentage sand
Si	%	Mass percentage silt
OC	%	Mass percentage organic matter
CEC	meq/100 g soil	Cation exchange capacity
BD	g cm^{-3}	Dry bulk density
k	-	Number of factors in Morris experiment
p	-	Morris experiment levels
r	-	Number or runs in Morris experiment
μ	-	Average elementary effects
σ	-	Standard deviation elementary effects
μ^*	-	Average absolute elementary effects

t_{rain}	minutes	Rainfall duration
P	mm	Rainfall
N	-	Number of vegetation observations
f_{shrub}	-	Shrub fraction of field
f_{grass}	-	Grass fraction of field
D	mm d^{-1}	Drainage
ΔS	mm d^{-1}	Soil water storage change
S	mm	Soil water storage
k_{ET}	d^{-1}	Reservoir model coefficient
S_{crit}	mm	Critical soil water storage
ET_p	mm d^{-1}	Potential crop evapotranspiration
K_c	mm d^{-1}	Crop coefficient
ET_a	mm d^{-1}	Actual crop evapotranspiration
K_{cb}	-	Basal crop coefficient
K_e	-	Soil evaporation coefficient
ET_{w0}	mm d^{-1}	Wet canopy evapotranspiration
K_{cf}	-	Crop factor
ET_{p0}	mm d^{-1}	Dry canopy evapotranspiration
E_{p0}	mm d^{-1}	Wet bare soil evaporation
K_{soil}	-	Soil evaporation factor
W_{frac}	-	Fraction of time that canopy is wet
P_i	cm h^{-1}	Intercepted precipitation
SC	-	Vegetative soil cover
$K_{cb,full}$	-	Basal crop coefficient full cover crop
F_r	-	Stomatal resistance correction factor
$K_{cb,h}$	-	Basal crop coefficient, full cover, subhumid, calm
RH_{min}	%	Mean minimum daily relative humidity
h	m	Vegetation height
r_l	s m^{-1}	Crop mean leaf resistance
$K_{c,min}$	-	Minimum crop coefficient
K_d	-	Density coefficient
$f_{c,eff}$	-	Effective fraction vegetation ground cover
M_L	-	Shade multiplier
ϕ	rad	Latitude
δ	rad	Solar declination
J	-	Day of year
T_p	mm d^{-1}	Potential transpiration
$K_{c,max}$	-	Maximum crop coefficient

$K_{c,field}$	-	Field crop coefficient
N_c	-	Number of crops
f_j	-	Fraction of field with crop j
h_j	m	Height of crop j
$K_{cb\ j}$	-	Basal crop coefficient of crop j
y	-	Output of interest
$\mathbf{x}$	-	k-dimensional vector holding model factor values
$\mathbf{x}^{(l)})$	-	Morris experiment sampling point
$\mathbf{x}^{(l+1)}$	-	Second Morris experiment sampling point
$d_i(\mathbf{x}^{(l)})$	-	Elementary effect for factor i
Δ	-	Morris experiment input change
$\mathbf{B}$	-	$(k+1) \times k$ strictly lower triangular matrix of ones
$\mathbf{x}^*$	-	Vector containing random factor values
$\mathbf{D}^*$	-	Diagonal matrix with diagonal elements 1 or -1
$\mathbf{J}_{k+1,k}$	-	$(k+1) \times k$ matrix of ones
$\mathbf{J}_{k+1,1}$	-	$(k+1)$ column matrix
$\mathbf{P}^*$	-	$k \times k$ random permuation matrix
$\mathbf{B}^*$	-	$(k+1) \times k$ dimensioned matrix containing one Morris trajectory
$x^o_v(z)$	-	Coordinate in a point in a Morris trajectory
$D_{m,o,p}$	-	Distance among three Morris trajectories
$\mathbf{V}^*$	-	$(k+1) \times k$ matrix containing SWAP inputs
κ_{upper}	-	Upper bound of experimentation in Morris experiment
κ_{lower}	-	Lower bound of experimentation in Morris experiment
$\mathbf{K}_{k+1,k}$	-	$(k+1) \times k$ matrix with each element κ_{lower}
$\mathbf{M}$	-	k-dimensional diagonal matrix holding midpoint SWAP inputs

1 INTRODUCTION

1.1 PROBLEM DESCRIPTION

Groundwater is an important resource of potable water: it amounts to 97% of the world's fresh water (Gleick et al., 1993), and a large part of the global population depends on it. Groundwater recharge rates play a role in the occurrence of freshwater lenses beneath islands, overlying saline groundwater (Fetter, 1972). When carefully managed, these lenses provide relatively easy access to fresh water. Groundwater also acts as a medium transporting solutes through the subsoil and is an important factor to consider in pollution management. Groundwater may transport solutes and nutrients from landfills and saniation pits to coastal aquatic ecosystems. These ecosystems suffer strongly from eutrophication: increasing turbidity, extinction of fish species, dying coral reefs, and emerging toxic phytoplankton species are among the expected effects (Pinto-Coelho et al., 2005; Howarth and Marino, 2006; Martinelli et al., 2006).

Quantifying long term groundwater recharge is crucial in effective groundwater management. Groundwater recharge is generally considered to be the downward, vertical flow of water across the water table that replenishes the aquifer, but it may also include flow between underlying or adjacent aquifers; in this research, recharge is defined as the downward water movement across a water table. While groundwater recharge is an extremely important component in groundwater studies, it is often difficult to characterize as recharge rates vary strongly in space and time. Additionally, rates are very difficult to measure directly.

St. Eustatius lacks good waste disposal infrastructure and waste water disposal infrastructure, with municipal solid waste being dumped at an open landfill and waste water discharging untreated or partially treated into pits (Van der Velde et al., 2010). These sanitation systems can pose a threat to public health, with pathogens sometimes travelling over 1 km in the groundwater (Dillon, 1997). Nutrients from these pits will also be transported to the coastal ecosystems. There are plans to expand agricultural land by 15 hectares, which would involve an additional fertilizer load for the ecosystem although the National Marine Park is an important tourist attraction (Van der Velde et al., 2010).

No previous estimations of groundwater recharge on St. Eustatius exist. Other researchers have investigated groundwater on other volcanic andesitic islands in the Caribbean Sea. Charlier et al. (2011) in-

vestigated an andesitic aquifer on Gaudeloupe and found that the aquifer recharge is about 59% of the rainfall for an average rainfall year, while Rad et al. (2007) estimated using analysis of chemical weathering that infiltration represents 10% of rainfall on Guadeloupe and 40% of rainfall on Martinique. The large difference may be explained by the small research area of Charlier et al. (2011), which features a highly permeable aquifer. Average yearly rainfall is much higher on these islands than on St. Estatius, however, so that fractions like these are effectively incomparable. Veenenbos (1955) performed a soil and land capability survey. Augustinus et al. (1985) updated this research, and also investigated vegetation types. Westermann and Kiel (1961) have described the geology, and more recently Roobol and Smith (2004) investigated the geology greater detail. Vegetation was investigated several times, most recently by De Freitas et al. (2012).

In 2013 the case study *Zero nutrient discharge and total reuse of nutrients* (Wageningen UR, 2013) was started by Wageningen UR, with a sub-objective 'to quantify the nutrient flows within and to and from the island, including nutrient losses to the marine environment through erosion and run-off'. This MSc thesis intends to assist in fulfilling the objective of quantifying the nutrient flow via groundwater from the island. The quantity of groundwater discharging into the ocean cannot be estimated directly, but under the assumption of steady-state discharge is equal to inflow, groundwater recharge, which can be estimated. On this basis a first attempt can be made at quantifying groundwater recharge and groundwater discharge into the ocean. The main research question is:

- What is the long term groundwater recharge on the Cultuurvlakte of St. Eustatius?

Additionally, the following questions are addressed:

- Which hydrological processes are the most important in generating recharge on St. Eustatius: to which SWAP inputs is simulated groundwater recharge the most sensitive?
- Under which conditions is groundwater recharge generated on St. Eustatius?
- What is needed to improve estimates of groundwater recharge on St. Eustatius?

1.2 SITE DESCRIPTION

Sint Eustatius, English Saint Eustatius, is one of the Leeward Islands in the northeastern Caribbean Sea, belonging to the Lesser Antilles, see figures 1 and 2. The island is located between 17°28′ and 17°32′ N latitude and between 62°56′ and 63°0′ W, 26 km southeast of Saba,

and 13 km northwest of St. Kitts. The island has a surface area of circa 21 km², a greatest length of 8 km and a greatest width of 4 km. It has a population of just over 4000 inhabitants (Centraal Bureau voor de Statistiek, 2014).

St. Eustatius is an andesitic volcanic island, and consists of three units, geologically speaking. The Northern hills are what is left of an extinct volcano system. The Quill and the Cultuurvlakte are in fact one geological unit, as the Cultuurvlakte is simply the base of the Quill volcano. This unit exists almost entirely of pyroclastic materials. The third geological unit is the White Wall-Sugar Loaf ridge, which forms a part of the Quill on the south shore and which has been identified as uptilted shallow-water limestone. The Quill is the youngest geological unit on the island. Its formation started around 50,000 years ago, with the uppermost part of the Quill dating as recent as circa 1600 years before present. The limestone formation is of intermediate age, and has been formed from 320,000 to 68,000 B.P. The White Wall-Sugar Loaf formation was then lifted upwards by the rise of the volcanic dome. The oldest unit is the group of extinct volcanic domes of the northern hills, with materials dated to around circa 500,000 years ago (Roobol and Smith, 2004). See figure 3 for a cross-section.

St. Eustatius can be divided into three distinct landscapes (Westermann and Kiel, 1961). The north consists of a hilly landscape (tops 200-300 meters above sea level (a.s.l.)) and the south is characterized by a single volcano, the Quill, peak at 600 m a.s.l. A sloping plain, the 'Cultuurvlakte', stretches out in between, dipping in northerly direction with elevations ranging from 30 to 80 m a.s.l., averaging 40 m a.s.l. See figure 4.

According to De Freitas et al. (2012) precipitation occurs with an annual average of 986 mm. August, September, October, and November are the wettest months, accounting for 47% of the long term annual average rainfall. Averages on the Quill may be as high as 1500–2000 mm according to Veenenbos (1955), caused by orographic effects; with rain forming as air is forced upwards by the slopes of the Quill. No rain gauges are located above 400 m a.s.l., so this remains unconfirmed by quantitative data (De Freitas et al., 2012). The surface water streams on St. Eustatius are ephemeral, flowing only during and after heavy rainfall. They have eroded gullies into the slopes of the northern hills and the Quill (Palm, 1985). Temperature is constant all year round, averaging at 27 °C. The vegetation consists primarily of thorny woodland and grassland on the Cultuurvlakte and the northern hills. Elfin forest is found on the highest part of the Quill's rim, and evergreen seasonal forest in the crater (Rojer, 1997).

For the purpose of the analysis, St. Eustatius is schematized as follows (figure 5): Precipitation occurs uniformly over the island. A part of the precipitation percolates and recharges a connected uncon-

Figure 1: Map of the Caribbean. Made with Natural Earth. Free vector and raster map data at naturalearthdata.com.

Figure 2: Map of part of the Leeward Islands. Free vector and raster map data at naturalearthdata.com.

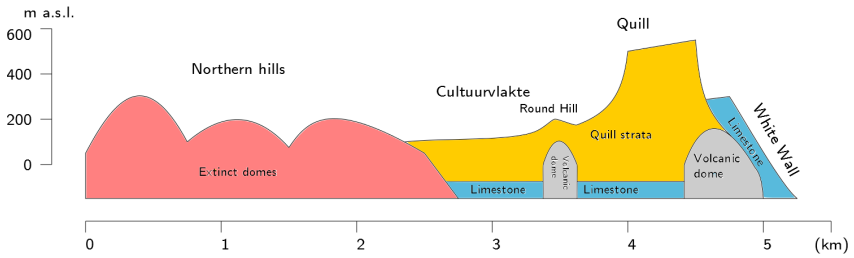

Figure 3: North-south geological cross section of St. Eustatius. Adapted from Westermann and Kiel (1961).

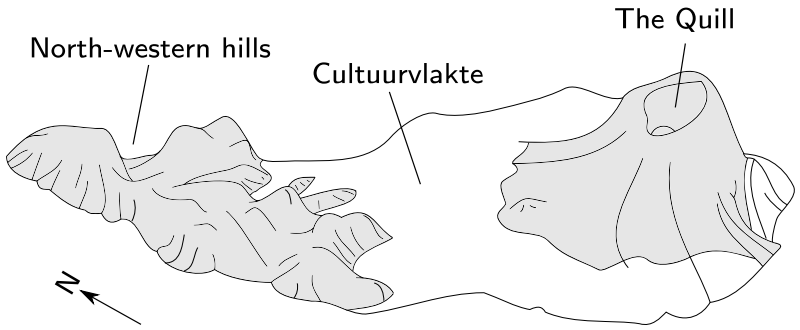

Figure 4: St. Eustatius landscapes. Adapted from Augustinus et al. (1985).

fined aquifer underlying the Cultuurvlakte. Precipitation occurring on slopes facing away from the Cultuurvlakte are assumed to have no contribution to the recharge of this aquifer. Fairly high hydraulic conductivities and high elevation above sea level are responsible for the existence of a thick unsaturated zone. Hydraulic conductivities are also high enough to prevent perched groundwater aquifers from forming, unlike the Hawaiian model described by Lachassagne et al. (2014), which features perched aquifers on top of volcanic dykes. Most of the extracted groundwater is brackish (Palm, 1985), which suggests the freshwater lens is small. The Cultuurvlakte aquifer discharges into the ocean at the western and eastern coastline.

It is not clear how much of the island recharges the Cultuurvlakte aquifer. Subsequently, the study area has been delimited conservatively by including the northern flank of the Quill: if the groundwater follows the shape of the topography, groundwater flow on the northern part of the Quill is towards the Cultuurvlakte so that this part of the Quill also recharges the Cultuurvlakte (see figure 6).

1.3 APPROACH TO ESTIMATE RECHARGE

A wide range of approaches are available for estimating groundwater recharge. Healy (2010) identifies the following categories: modeling methods, surface-water data methods, physical methods involving

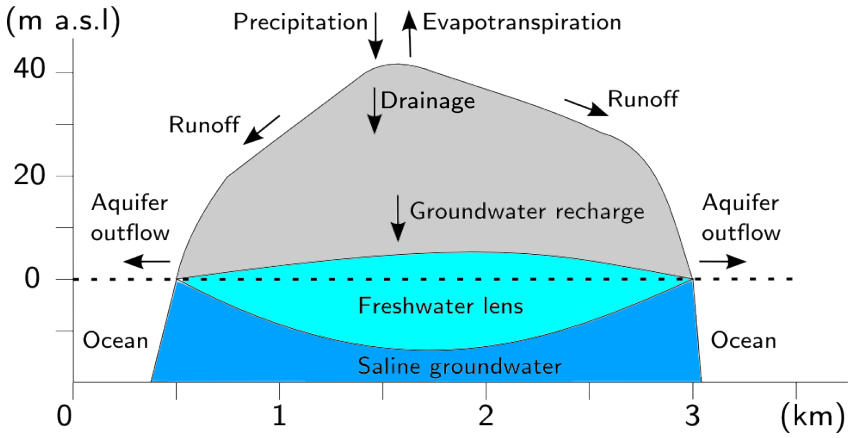

Figure 5: Conceptual hydrologeological model of the Cultuurvlakte aquifer. Vertical dimensions of the supposed freshwater lens are exaggerated.

the saturated zone, physical methods involving the unsaturated zone, and tracer methods. The need for a long term estimate of groundwater recharge and the lack of surface water disqualifies all these methods except for modeling. In terms of modeling, the lack of hydrogeological data further disqualifies modeling groundwater flow. The only method left is modeling of the unsaturated zone.

Assuming groundwater on St. Eustatius behaves as shown in figure 5, all water that recharges the water table passes through the unsatured zone. Groundwater recharge can then be estimated by calculating the quantity of water that leaves the unsaturated zone; this quantity can be calculated by simulating water flow in the unsaturated zone. Numerical models simulating water flow in the unsaturated zone like SWAP (Kroes et al., 2009) or HYDRUS-1D (Simunek et al., 2008) have been succesfully used for the purpose of estimating groundwater recharge, see for example Anuraga et al. (2006), Lu et al. (2011), Sarwar et al. (2000), Jiménez-Martínez et al. (2009), or Ahmad et al. (2002).

In this study, groundwater recharge was estimated using the 1D unsaturated zone model SWAP, version 3.2 (Kroes et al., 2009); SWAP was chosen for this study because of the expertise and familiarity that my supervisors have with it. SWAP, for *Soil-Water-Atmosphere-Plant*, describes a domain that spans from the top a vegetation canopy down to the groundwater table. It is used in this study to simulate the interception and evaporation of rainfall, infiltration and soil water flow, and vegetation root water uptake and transpiration. The resulting drainage flux at the bottom of the soil column is assumed to recharge the groundwater.

When rainfall occurs in SWAP, a part is intercepted by the vegetation canopy and evaporates and another part falls on the soil. Then, it either evaporates from there or it infiltrates and flows through the

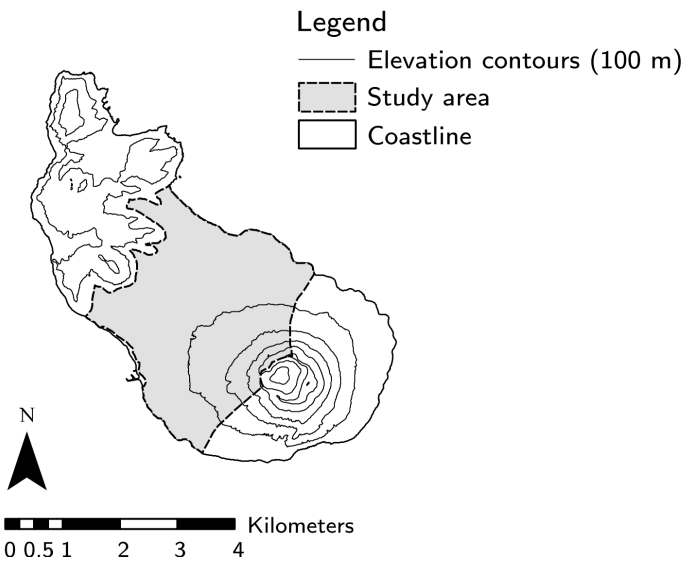

Figure 6: Map of the study area.

soil. Soil water flow is governed by the 1D Richards equation, which combines Darcy's equation for flow through porous media and mass conservation for a control volume as

$$\frac{\partial \theta}{\partial t} = \frac{\partial \left[K(h) \left(\frac{\partial h}{\partial z} + 1 \right) \right]}{\partial z} - S_a(h) \tag{1}$$

where θ (cm^3 cm^{-3}) is volumetric water content, t (d) is time, K is hydraulic conductivity (cm d^{-1}), h (cm) is soil water pressure head, z (cm) is the vertical coordinate taken positively upward. Driven by gravity, the water flows downward eventually leaving the simulated soil column, unless it is taken up by the vegetation as S_a (cm^3 cm^{-3} d^{-1}), plant root soil water extraction. Root water is dependent on the amount of water plants need to transpire, which is dependent on plant physiology and meteorological conditions. As soil pressure heads decrease, the plant experiences water stress and root water uptake is reduced. For a detailed description of SWAP, see the SWAP Theory description and user manual (Kroes et al., 2009).

The following inputs had to be determined: rainfall, meteorological conditions, vegetation parameters, and soil hydraulic parameters. The simulation period was set to 1983–2014 as this was the longest period over which meteorological data were available. How these inputs were estimated is explained the first four sections of the following chapter.

2

METHODS

2.1 RAINFALL AND METEOROLOGY

The F.D. Roosevelt airport on St. Eustatius has a meteorological station measuring air temperature, dewpoint, windspeed, air pressure, and precipitation. These data are available from NOAA's *Global Summary of the Day* service (National Oceanic and Atmospheric Administration, 2014). Records start in 1975, but the timeseries has many gaps: over a period of 40 years, less than half of the days have records. Over the 30 year period 1984 to 2014, only 59% of the days have records; for the period 1994 to 2014, 71%. This renders this dataset unsuitable for calculating groundwater recharge, especially if we consider that potentially up to a third of the precipitation has gone unrecorded.

The measurements from Robert Bradshaw airport on St. Kitts are also available on *Global Summary of the Day*. The timeseries from St. Kitts has far fewer gaps: for the period 1984 to 2014, 92% of days have been recorded. The distance between the airports of St. Eustatius and St. Kitts is 35 km, so the climate should be comparable.

From June 1980 to 2006, mrs. Taylor, a resident of St. Eustatius, has also measured rainfall daily at Upper Round Hill on the northwestern slope of the Quill. However, the measured values were recorded only four times per month, exact dates unknown (Shelley Works, personal communication, October 2014). Effectively, the timeseries has a monthly resolution. Mr. and mrs. Work continued the rain measurements from 2006 onwards at Pleasures, also with monthly resolution. With the installation of a Davis Weather Vantage Plus Pro station in January 2013 (George Works, personal communication, October 2014), precipitation data is available with a temporal resolution of 15 minutes, which has been increased over the last two years to a one minute resolution.

Finally, another dataset available is a list of average monthly rainfall sums in Braak (1935) for five stations, the longest timeseries running over a period of 53 years, from 1881 to 1933 in Oranjestad.

Suitability St. Kitts data

While St. Kitts and St. Eustatius are close and should experience the same climate, local conditions could affect measurements. St. Kitts is notably larger (176 km² versus St. Eustatius's 21 km²), but the airports are both located on flat stretches of land with a clear horizon in northeasterly direction. The airport of St. Kitts is enclosed by hills

and is surrounded by more land. Elevations are similar: 52 m a.s.l for the aiport of St. Kitts, and 39 m a.s.l for St. Eustatius.

For the purpose of estimating long term groundwater recharge, day to day differences between the locations are of little importance. It is more important that the long term weather, the climate, is the same. Means and histograms of average daily temperature, diurnal temperature range, relative humidity, and wind speed have been compared. For this, measurements were used of days in the period 01-01-1983 to 31-12-2013 that were present in both timeseries from *Global Summary of the Day*. For precipitation, the monthly sums derived from *Global Summary of the Day* for St. Kitts and from the timeseries of Taylor and Works have been compared.

Rainfall duration

Rainfall duration can vary strongly for similar daily rainfall sums – a drizzle that lasts a day might precipitate as much as a heavy shower does in one hour. Accordingly, processes such as e.g. infiltration and evapotranspiration will behave differently under different rainfall intensities. To accomodate, SWAP has the option of including rainfall duration when using precipitation data with a daily resolution. This is useful for St. Eustatius, since its tropical climate indeed brings rainfall primarily as (short-duration) showers.

The 30 year timeseries only has data on daily precipitation sums, without rainfall duration. However, a relationship between rainfall sum and rainfall duration was found with non-linear regression on the rainfall measurements provided by the weather station of mr. and mrs. Works. I applied a cross-validation scheme to assess performance robustly. The dataset was randomly divided into two parts. The model was trained on the first part, and the determined coefficient values were subsequently validated against the second part of the dataset. This was repeated a thousand times, each time randomly re-dividing the dataset. For the final use of estimating rainfall duration, the model was calibrated using the entire dataset.

The tipping bucket rainfall gauge initially recorded the amount of rainfall every 15 minutes. Later, it recorded every 5 minutes and finally every 1 minute. These periods have been used as the duration of the rainfall. This results in some errors early in the timeseries: rainfall that fell in only a minute is interpreted as rainfall that fell over the course of 15 minutes. To find a relationship between daily rainfall sums and daily rainfall duration, the rainfall and duration data have been aggregated to daily values. For example, if in one day on three occasions 1 mm of rain fell in 15 minutes, the aggregated rainfall will amount to 3 mm and the aggregated duration to 45 minutes.

The effects of this approach have also been tested in SWAP, by simulating the year of 2013 twice and comparing the results on recharge:

once with 15 minute rainfall data, and once with aggregated rainfall sums with modeled rainfall duration.

2.2 REFERENCE EVAPOTRANSPIRATION

Reference evapotranspiration is the combined rate of evaporation and transpiration from a reference surface, generally short grass (Allen et al., 1998). This rate is multiplied by a crop factor to estimate evapotranspiration of specific crops. There are many methods available for estimating reference evapotranspiration from meteorological data. These methods can be divided into temperature methods, radiation based methods, and mass-transfer methods (Tabari et al., 2013). Of these methods, those based on the Penman-Monteith equation are considered to be most accurate. The Penman-Monteith equation captures most physical processes involved in evapotranspiration. This does come with a price, namely the many inputs required: solar radiation, air temperature, relative humidity, and wind speed. In contrast, a simpler temperature method such as the Hargreaves-Samani (Hargreaves and Allen, 2003) equation requires only data on air temperature. However, the Hargreaves-Samani equation is not very accurate and is unsuitable for describing evapotranspiration on a daily scale. Rather, it should be used for time steps of five days or longer (Hargreaves and Allen, 2003). Therefore, the FAO Irrigation and Drainage Paper No. 56 (Allen et al., 1998) (hereafter called FAO-56) recommends applying the Penman-Monteith method even when not all inputs are available. FAO-56 also supplies methods for estimating these inputs where missing.

For St. Eustatius (or more precisely: for the airport of St. Kitts) long timeseries of air temperature, relative humidity, and wind speed are available from *Global Summary of the Day*. Solar radiation is not measured at the airport of St. Kitts, but is measured by the weather station of mr. and mrs. Works. Measurements of this weather station started at the 13th of January 2013, which provides two years of solar radiation data for analysis.

Solar radiation

FAO-56 recommends estimating solar radiation in one of the following ways. First, the Hargreaves radiation formula

$$R_s = K_{Rs}\sqrt{\Delta T}R_a \tag{2}$$

where R_s (MJ m^{-2} d^{-1}) is daily solar shortwave radiation, K_{Rs} (°C$^{-0.5}$) is an empirical coefficient, $\Delta T = T_{max} - T_{min}$ is the diurnal temperature range with T_{max} (°C) maximum air temperature and T_{min} (°C) minimum air temperature of the day, and R_a (MJ m^{-2} d^{-1}) is extraterrestrial radiation. K_{Rs} ranges from 0.16 to 0.19 for inland and

Table 1: Various radiation estimation models for the period 13-01-2013 to 13-01-2015. R_s is solar radiation; ΔT is diurnal temperature range; RH is relative humidity; R_a is extraterrestrial solar radiation; T is average daily temperature; W is 1 for days with more than 1 mm rain and 0 for days without; K_{Rs}, K_1, K_2, K_3, and K_4 are empirical coefficients. See the following chapter for model performance.

Model	Equation
Hargreaves	$R_s = K_{Rs}\sqrt{\Delta T}R_a$
Bristow-Campbell	$R_s = T_{t,max}(1-\exp(-C_1\ \Delta T^{C_2}))R_a$
M1	$R_s = (K_{Rs}\sqrt{\Delta T})R_a + K_1$
M2	$R_s = (K_{Rs}\sqrt{\Delta T} - K_1 RH + K_2)R_a$
M3	$R_s = (K_{Rs}\sqrt{\Delta T} - K_1 RH + K_2)R_a + K_3$
M4	$R_s = (K_{Rs}\sqrt{\Delta T} - K_1 RH + K_2\ T + K_3)R_a + K_4$
M5	$R_s = (K_{Rs}\sqrt{\Delta T} - K_1 RH + K_2 W + K_3)R_a + K_4$

coastal locations respectively. This equation is not suitable for island locations, because the surrounding water body may strongly influence temperature by temperature advection. This weakens the relation between temperature range and solar radiation. Instead, FAO-56 recommends an empirical method for island locations

$$R_s = 0.7\ R_a - b \tag{3}$$

where b (MJ m^{-2} d^{-1}) is an empirical constant with a value of 4, which may be adjusted for local conditions. However, this method is appropriate only for *monthly* calculations. Methods converting daily sunshine duration to solar radiation values (e.g. Suehrcke (2000)) cannot be used since sunshine duration data do not appear to be available for St. Eustatius or nearby locations.

Here, the two years of radiation data give an opportunity to estimate solar radiation more accurately. Equation (2) holds true to a degree: correlation between daily solar radiation and diurnal temperature range is 0.64. Additionally, correlation between daily solar radiation and relative humidity is -0.59. The negative correlation between daily solar radiation and relative humidity may be explained by the fact that on average a higher relative humidity leads to more clouds and less solar radiation.

Another common method for estimating solar radiation is the Bristow-Campbell model. The original Bristow-Campbell model (Bristow and Campbell, 1984) estimates radiation using

$$R_s = \tau_{max}(1-\exp(-C_1\ \Delta T^{C_2}))R_a \tag{4}$$

where τ_{max} (-) is the maximum transmittance, and C_1 ($°C^{-C_2}$) and C_2 (-) are empirical coefficients. Additionally, ΔT is corrected for wet days. While more numerically complex, the advantage of this method

over the Hargreaves formula is the asymptote: $(1 - \exp(-C_1\ \Delta T^{C_2}))$ cannot exceed 1, then R_s/R_a cannot exceed τ_{max}, so that τ_{max} has an easily interpreted physical meaning as the maximum transmittance under a clear sky (generally with a value of around 0.75).

Several models have been evaluated, including the Hargreaves and Bristow-Campbell models, and modified Hargreaves models. See table 1. Model performance was evaluated by applying the same cross validation scheme used for the rainfall duration model: by training and validating a thousand times, each time randomly re-dividing the dataset in two parts.

Options for reference evapotranspiration

Two methods for calculating reference evapotranspiration were tested. The first is the Hargreaves-Samani equation (FAO-56)

$$ET_{ref} = 0.0023(T + 17.8)\Delta T^{0.5} R_a \tag{5}$$

where T (°C) is the mean daily air temperature at 2 m height. The second is the FAO Penman-Monteith equation (FAO-56)

$$ET_{ref} = \frac{0.408\Delta_v(R_n - G) + \gamma \frac{900}{T + 273} u_2 (e_s - e_a)}{\Delta_v + \gamma(1 + 0.34u_2)} \tag{6}$$

where ET_{ref} (mm d^{-1}) is reference evapotranspiration, Δ_v (kPa $°C^{-1}$) is the slope of the vapour pressure curve, R_n (MJ m^{-2} d^{-1}) is the net radiation at the canopy surface, G (MJ m^{-2} d^{-1}) is the soil heat flux, γ (kPa $°C^{-1}$) is the psychrometric constant, u_2 (m s^{-1}) is the wind speed at 2 m height, e_s (kPa) is the saturation vapour pressure, and e_a (kPa) is the actual vapour pressure. Δ_v, R_n, G, γ, e_s, and e_a were determined using the methods in FAO-56; and G is assumed negligible over a day. This equation describes evapotranspiration for a reference crop that is actively growing and adequately watered, with an assumed height of 0.12 m, a surface resistance of 70 s m^{-1}, and an albedo of 0.23.

For comparing methods, reference evapotranspiration with was calculated for the two years with existing solar radiation measurements; reference evapotranspiration has been calculated three times for the two year period, using:

1. the FAO Penman-Monteith method using measured solar radiation,
2. the Hargreaves method,
3. the FAO Penman-Monteith method using solar radiation estimated with the best model in table 1.

The results of the latter two were compared with the first, which is assumed to estimate evapotranspiration the most accurately.

2.3 VEGETATION

In SWAP, vegetation is central in three processes: evapotranspiration, root water extraction, and rainfall interception. The study area was divided into 18 *landscape units* of roughly half a square kilometer for the vegetation inventory, see figure 8. The land cover within a landscape unit is distinctly different from its neighbouring units (e.g. dominated by shrubs versus dominated by grass). The units were subsequently classified into a set of broad classes with the aid of satelite images (Bing Maps, 2014), a land cover map of St. Eustatius (Smith et al., 2013), and observations in the field. The assumption is that while vegetation changes over the course of the study period, the land cover class overall stays more or less the same. These classes are:

- Pasture: vegetation is nearly exclusively grass. This cover is found almost exclusively on the eastern coast of the island. None of the pastures are fenced and most of the grass is kept short by grazing animals.
- Airport: also exclusively grass (except for the runway) but free from grazing, as it is fenced off. The grass is mown so that the vegetation length is relatively constant; it is assumed to evapotranspire like the FAO-56 reference grass.
- Shrubland: the most common land cover on St. Eustatius. It is a mixture of primarily grasses and thorny shrubs, which range in height from 1 to 5 m.
- Forest: can only be found the higher parts of the Quill. It does not feature much understorey vegetation, and maximum average height amounts to 6 to 8 m.
- Built-up: features most of the houses and buildings on the island, the gardens and areas between houses and the immediate area surrounding the houses and building. This class is very heterogeneous: it consists of roofs, roads, lawns, but also a variety of shrubs and trees in gardens. The non-paved area in this class is treated as shrubland, which is most similar of the investigated classes, also consisting of herbaceous and woody vegetation of various heights.

See figure 7 for examples. The vegetation itself was classified into four categories: pasture grass, shrubland grass, shrubland shrubs, and forest.

Pasture

Airport

Shrubland

Forest

Built-up

Figure 7: Pictures of the five land cover classes in the study area.

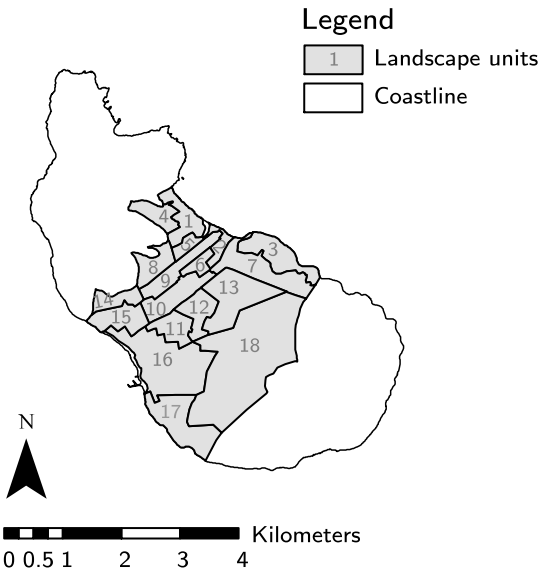

Figure 8: Study area divided into 18 landscape units.

Crop factors

For estimating evapotranspiration from reference evapotranspiration, crop factors are required. Crop factors provide a convenient way of accounting for crop type and phenology. An extensive list of crop factors is given by FAO-56 for agricultural crops. However, almost no crop factors have been determined for natural vegetation and no list of crop factors for semiarid (natural) vegetation is available. FAO-56 presents a calculation procedure for the crop factor based on leaf area index or vegetation height and vegetative soil cover for natural, non-typical, and non-pristine vegetation. On St. Eustatius, a negligible amount of land is used for agricultural crops. Most of the vegetation on the study is natural (although heavily anthropogenically disturbed (De Freitas et al., 2012)) and non-pristine. With this method, a crop factor has been estimated which is converted and then used as the crop factor in SWAP. A detailed description of how the crop factors have been calculated can be found in appendix A.

The fieldwork took place over the course of two weeks in December, at the end of what is generally the rain season. Soil cover was determined visually from photographs with the aid of comparison charts. For grass and herb vegetation, the photos were taken 2 m above the ground, the camera pointing straight downwards. Photos of the canopy were taken from from the ground surface, the camera pointing straight up. Care was taken that vegetation cover was estimated from the center of the photos, to avoid non-vertical sighting bias. Photos

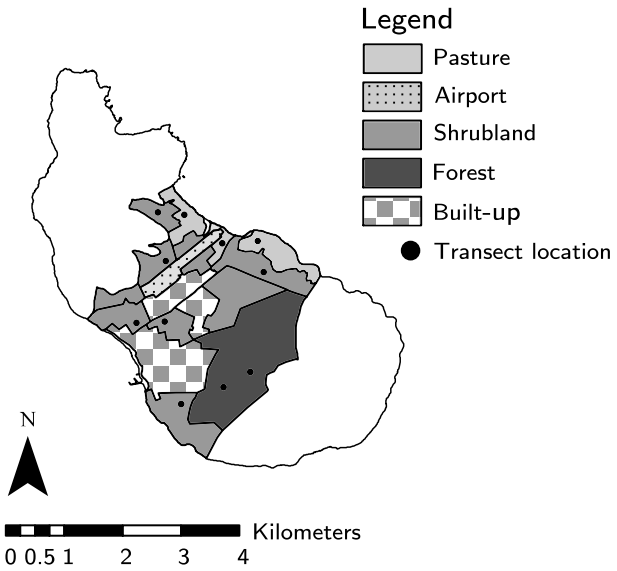

Figure 9: Locations of vegetation sampling transects in the landscape units of the study area, with land cover classes.

were mostly taken in overcast conditions, as harsh shadows made analysis more difficult.

Average maximum vegetation height was assessed with a 2 m measuring stick. Vegetation taller than 2 m was measured by marking the 2 m height, and raising the stick above that, and reading the vegetation height from the ground. The height of vegetation taller than 5 m (extending the reach of my arm and measuring stick) was estimated by visual comparison.

Figure 9 shows the location of the sampling sites. I measured vegetation along transects as well as I could (in sometimes thorny shrubland) to avoid subjective sampling of vegetation, sampling vegetation every twenty steps. I selected representative locations for these transects, that is, transect locations that appeared representative for the landscape unit as a whole in terms of canopy density and vegetation height. Measuring the extremely heterogeneous vegetation of the built-up areas was outside of the scope of this research.

Rooting depth

Rooting depth was observed at soil profile pits, but it proved very difficult to get good estimates for trees and shrubs. Therefore, the rooting depths of trees and shrubs have been taken from a global dataset (Schenk and Jackson, 2002). The values were taken for a location that has similar sums of mean annual rainfall and reference evapotranspiration: for forest, data from Puerto Rico has been used; for shrubland, data from Uttar-Pradesh, India. The dataset provides

two depths, D50 and D95, which are the depths in m above which respectively 50% and 95% of all roots were located in the soil. The D95 has been used as the maximum rooting depth. Schenk and Jackson (2002) fitted an equation to cumulative root profiles. When differentiated, this equation gives root density as a function of relative depth, and has the form

$$r_d = \frac{-c_r \left(\frac{D50^*}{D^*}\right)^{c_r}}{\left(\left(\frac{D50^*}{D^*}\right)^{c_r}\right)^2 + 1} \tag{7}$$

where r_d (-) is root density, c_r (-) is a shape parameter, D^* (-) is relative rooting depth defined as $D^* = D/D95$ with D (m) depth below the surface, and $D50^*$ (-) is the relative D50 defined as $D50^* = D50/D95$. The rootzone distributions for shrubland and forest have been calculated with equation (7). The rootzone distribution for pasture was estimated visually in the field – a precise excavation and inventory of plants roots was outside of the scope of this research.

Interception and root water extraction

SWAP has two interception models available: the Von-Hoyningen-Hüne and Braden model, which is appropriate for agricultural vegetation, and the Gash model for forests. An important conceptual difference between these models is that the first model does not simulate evaporation from a wet canopy and that the Gash model does (greater roughness results in a smaller aerodynamic resistance, and more evaporation) (Kroes et al., 2009). Measuring rainfall interception was outside of the scope of this research. The literature was searched instead for parameter values, but no reliable estimates could be found. For these parameters, SWAP defaults were used instead. Nevertheless, to evaluate their importance, the parameters have been included in two sensitivity analyses: in the first sensitivity analysis the Von-Hoyningen-Hüne and Braden model was used for simulating interception and in the second sensitivity analysis the Gash model.

For the woody shrub vegetation, some Gash interception parameters were found: Návar and Bryan (1994), Návar et al. (1999a) and Návar et al. (1999b) fitted the Gash model for shrubs in northern Mexico, but they report a very wide range of values. Additionally, a major challenge is scaling up interception observations from single shrubs to landscape units, with patches of grass between the shrubs. These values have been used as baseline values in the second sensitivity analysis. These values were also used in a few test simulations, to get an impression of the effects of interception.

Root water extraction parameters were left at defaults values for identical reasons, and were also included in the sensitivity analyses.

2.4 SOIL HYDRAULIC PROPERTIES

For this study, the soil hydraulic properties are described in SWAP using the Mualem-Van Genuchten functions

$$\theta(h) = \theta_r + \frac{\theta_s - \theta_r}{[1 + (\alpha|h|)^n]^{1-1/n}} \tag{8}$$

$$K = K_s S_e^{\lambda}[1 - (1 - S_e^{1/m})^m]^2 \tag{9}$$

where θ_s ($cm^3\ cm^{-3}$) is the saturated water content, θ_r ($cm^3\ cm^{-3}$) is the residual water content, and α (cm^{-1}), n (-), m (-) are empirical shape factors that depend on soil type, K_s ($cm\ d^{-1}$) is the saturated hydraulic conductivity , λ (-) a shape parameter, and S_e (-) is relative saturation. m is taken as

$$m = 1 - \frac{1}{n} \tag{10}$$

and S_e is defined as

$$S_e = \frac{\theta - \theta_r}{\theta_s - \theta_r} \tag{11}$$

Consequently, the parameters required are residual water content θ_r; saturated water content θ_s; shape parameters α, n, and λ; and saturated hydraulic conductivity K_s.

θ_s and K_s have been determined in the field as they can be measured with simple equipment. The other parameters have been generated with a pedotransfer function and λ has been set to a value of 0.5 (Mualem, 1976).

Field work

The soil was schematized into discrete layers using four soil profile pits in the field, and based on the description of Veenenbos (1955); see figure 10 for the soil map.

Dry bulk density and saturated water content were determined using 100 cm^3 soil sampling rings. 110 samples were taken in total, locations are shown in figure 11. Per location five samples were taken at the surface and five just below the surface, at a depth of 5–10 cm. The soil was generally hard and the rings had to be hammered in. After the sample had been dug out, filter paper was tied around the base of the rings with some string and they were saturated for 24 hours. Water was added in two phases to avoid trapping air: water was added first to half the height of the ring, then to full height. Afterwards, the ring were left briefly to drain excess water, weighed and placed in an oven for drying at 110-120 °C. After 24 hours the rings were weighed

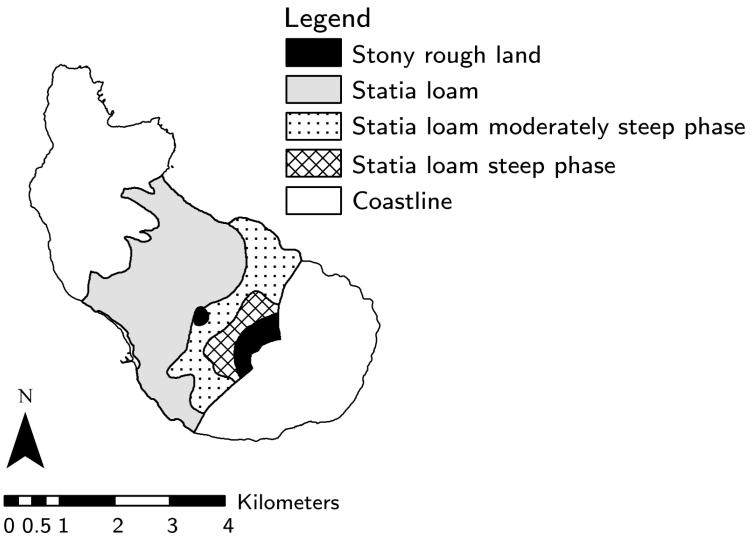

Figure 10: Soil map of the study area after Veenenbos (1955).

again to determine bulk density. Saturated water content was calculated using the difference between wet and dry weight. The empty rings, the filter paper, and the string were weighed dry and wet as well to correct for their weight. The rings with content were weighed with a scale with an accuracy of 1 gram. The empty rings, the filter paper, and the string were weighed with a scale with an accuracy of 0.01 gram (this scale had a maximum weight of 200 g and could not be used to weigh the full rings).

Saturated hydraulic conductivities of the soil were determined 67 times with a Decagon Devices Mini Disk Infiltrometer Model S (Decagon Devices, 2011) at the same locations at which the soil samples were taken. At every site, soil infiltration rates were measured both at the surface and just below the surface, at a depth of 5–10 cm. Another 46 conductivity measurements made by fellow student Wouter ten Harkel for his research (Ten Harkel, 2015) in the study area, have also been analyzed. Every measurement was conducted in triplo, amounting to six measurements per site. These 46 measurements are of the surface only. Measurements were analyzed using the method of Zhang (1997), as presented in the infiltrometer manual (Decagon Devices, 2011). A pit was excavated at location II in figure 18 to measure infiltration rates at depths of 20, 30, 40, and 110 cm.

Pedotransfer function

The water retention pedotransfer function developed by Hodnett and Tomasella (2002) for tropical soils was used to determine θ_r, θ_s, α, and n. For the sandy loam topsoil a continuous pedotransfer function was used. For the sandy subsoil, a look-up table in Hodnett and

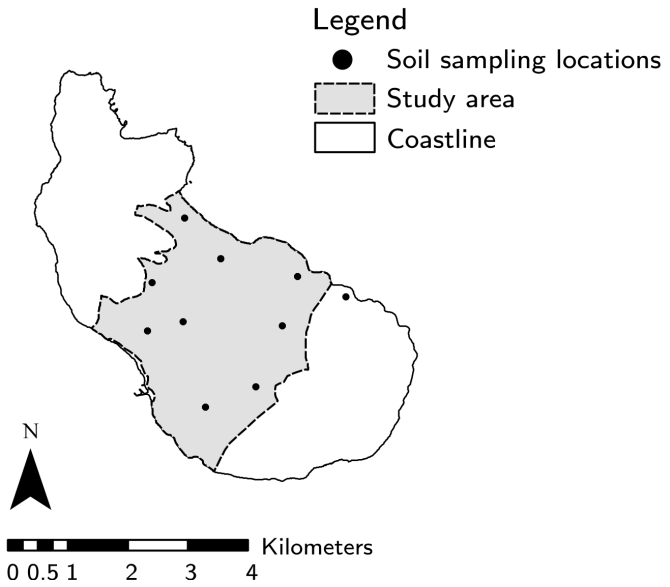

Figure 11: Soil sampling and infiltration experiment locations.

.

Tomasella (2002) was used instead because of a lack of data on this layer. The continuous pedotransfer functions for θ_r, θ_s, α, and n are

$$\theta_r = 0.22733 - 0.00164\ \mathrm{Sa} + 0.00235\ \mathrm{CEC} - 0.00831\ \mathrm{pH} + 1.8 \times 10^{-5}\ \mathrm{Cl}^2 + 2.6 \times 10^{-5}\ \mathrm{Sa} \times \mathrm{Cl} \quad (12)$$

$$\theta_s = 0.81799 + 9.9 \times 10^{-4}\ \mathrm{Cl} - 0.3142\ \mathrm{BD} + 1.8 \times 10^{-4}\ \mathrm{CEC} + 0.00451\ \mathrm{pH} - 5 \times 10^{-6}\ \mathrm{Sa} \times \mathrm{Cl} \quad (13)$$

$$\alpha = -0.02294 - 0.03526\ \mathrm{Si} + 0.024\ \mathrm{OC} + 7.6 \times 10^{-3}\ \mathrm{CEC} - 0.11331\ \mathrm{pH} \quad (14)$$

$$n = 0.62986 - 0.00833\ \mathrm{Cl} - 0.00529\ \mathrm{OC} + 0.00593\ \mathrm{pH} + 7 \times 10^{-5}\ \mathrm{Cl}^2 - 1.4 \times 10^{-4}\ \mathrm{Sa} \times \mathrm{Si} \quad (15)$$

where Cl, Sa, Si, and OC (%) are mass fractions for clay, sand, silt, and organic matter respectively; CEC (meq/100 g soil) is cation exchange capacity; and BD (g cm^{-3}) is dry bulk density. Average values for Cl, Sa, Si, OC, and pH were determined from the analyses of the sandy loam topsoil by Veenenbos (1955) and Augustinus et al. (1985), CEC from Augustinus et al. (1985), and average bulk density was determined using my own measurements.

2.5 SWAP SIMULATION

The results of the methods in the previous sections have been used to setup SWAP. Figure 12 presents an overview of how the input parameters for SWAP have been determined.

The simulated soil column had a depth of 300 cm. Free drainage was assumed as the bottom boundary condition, which is justified (Carrera-Hernández et al., 2012) given the very deep groundwater levels. Hysteresis in the water retention curve has been ignored, as as well as macropore flow. To avoid runoff, the ponding depth needed for the generation of runoff has been set to a very high value (1000 cm). In reality runoff does occur, but generally locally. The assumption here is that the runoff generally infiltrates close to where it it generated, so that for the water balance of a simulation unit the runoff that leaves the simulation unit is negligible. It is outside of the scope of this research to simulate the precise effects of runoff. For example, roads are especially likely to generate runoff, but this runoff does disappear from the study area. There are several infiltration areas in the study area, designed specifically to let the runoff from the roads infiltrate. This has not been modeled, the roads have been left out of the simulation. The findings of Ten Harkel (2015) justify this approach: net runoff losses amount to a few percentage of rainfall.

The model had a burn-in time of four years: the model ran simulations from 1 January 1980 to 31 December 2013, but only the 30 year period from 1 January 1984 to 31 December 2013 was analyzed to determine groundwater recharge. Initial conditions were generated as follows: first, uniform pressure head inital conditions were set to a value of -10000 cm. Second, a simulation was run using these conditions. Third, the end results of this simulation were used as the initial conditions for the actual simulations.

2.5.1 *Sensivity analysis*

A sensitivity analysis was performed to gain insight into which inputs are the most important in determining recharge, and to determine how the study area should be represented in discrete simulation units for SWAP. A global sensitivity analysis was performed using the Morris method (Morris, 1991). The Morris method is a screening design requiring a relatively small number of model runs to estimate for a selected output the sensitivity to its inputs (here called factors). It is a one-factor-at-a-time method, i.e. only one input is changed between model runs. The change in the output due to the change in a particular factor is called an *elementary effect.* For a k number of factors, each factor may assume a discrete number p of values, called *levels*. The method essentially does a great number of sensitivity analyses, one for each parameter. Doing these separately would require two sim-

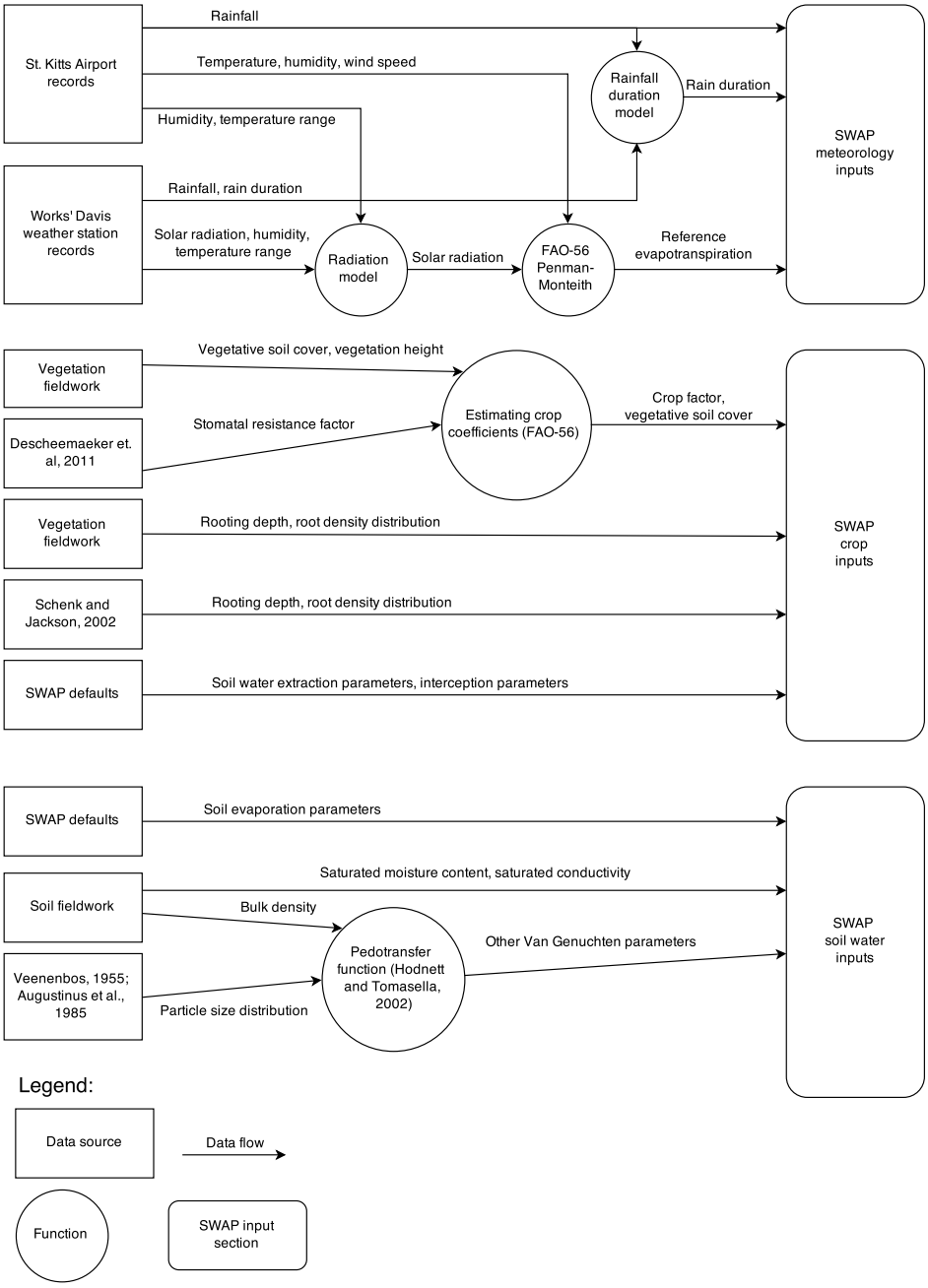

Figure 12: Data flow diagram for the SWAP inputs.

ulations per parameter (2k), but by chaining them together a much greater efficiency can be achieved ($k + 1$). The method consists of a series of randomized *trajectories* through the input space. Every point and its neighbouring point in the trajectory provide one elementary effect. An r number of trajectories is evaluated, thereby providing r elementary effects per input. For each trajectory, the starting point and the order in which the inputs are varied are random. Sensitivity can be then be expressed per input as the average of the elementary effects (μ), the standard deviation (σ), and the average of the absolute elementary effects (μ^*). These are interpreted as follows:

1. A large μ^* suggests sensitivity to the factor, a low μ^* suggests insensitivity.

2. A large σ suggest a nonlinearity or interaction with other factors, whereas a low σ suggests linearity and lack of interaction.

3. A high μ^* but a low μ suggests non-monotonicity, as it results in cancellation of terms of different signs for μ but not for μ^*.

See figure 13 for a visual example, showing a step-by-step construction of a trajectory.

Campolongo et al. (2007) proposed an improved sampling design. This consist of selecting trajectories in such a way that they are maximally spread in the input space. After all, the sensitivity analysis is local rather than global when all trajectories are located in the same corner of the input space. For a detailed description of the methods used to generate and select optimal trajectories, see appendix B. Following the recommendations of Campolongo et al. (2007), $r = 10$ trajectories were used in the sensitivivity analysis with $p = 4$ levels; so that for every factor μ, μ^*, and σ were calculated using 10 elementary effects.

Ideally, sensitivity is investigated in the relevant population of the factors. Assuming we know the probability distributions of all factors, we might (arbitrarily) select quantiles, say the 20^{th} and 80^{th} percentile. These percentiles are transformed to actual parameter values using the probability distribution of that parameter. It is in the space bounded by these upper and lower values that the sensitivity analysis is performed (Saltelli et al., 2004). For this study the distributions of only two parameters are approximately known, topsoil saturated water content θ_s and topsoil saturated hydraulic conductivity K_s. Hence, the Morris experiment here was performed first using a perturbation of maximally 15% around a baseline value for each factor ($\kappa_{upper} = 1.15$, $\kappa_{lower} = 0.85$). With four levels, values are perturbed by 0.85, 0.95, 1.05, and 1.15. The factors that were varied in the sensitivity analysis are shown in table 3, along with the baseline value for each factor. The baseline values are the values found for shrubland. A second sensitivity analysis was performed using the

1. Choose the factors for the sensitivity analysis. Set up the area of experimentation and set up a grid. This example uses two parameters: x_1 and x_2.

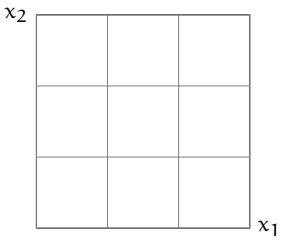

2. Choose a random grid point. This is the start of the trajectory. Simulate using the values of x_1 and x_2 and generate model output y.

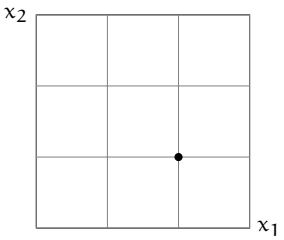

3. Randomly select an input to change; here it is x_2. Simulate using the changed inputs to generate another model output.

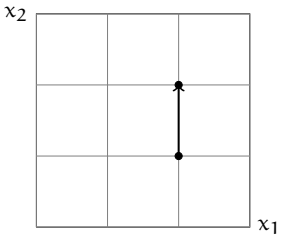

4. Compare the results of the simulations. The difference caused by altering x_2 is called an elementary effect for x_2: Δy_{x_2}.

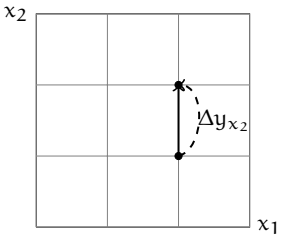

5. Again, randomly select a parameter (that has not been changed yet); in this case only x_1 is left. Simulate using the changed inputs to generate a third model output.

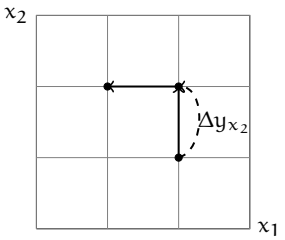

6. Compare the results of the simulations. The difference caused by altering x_1 is called an elementary effect for x_1: Δy_{x_1}. When all inputs have been changed and an elementary effect is calculated for every input, the trajectory is finished.

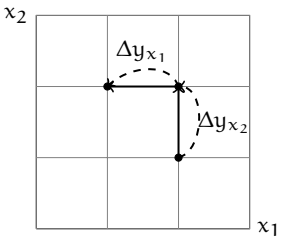

More trajectories can be constructed to give a set of elementary effects per input. Then for each input, the μ, μ^*, and σ can be calculated.

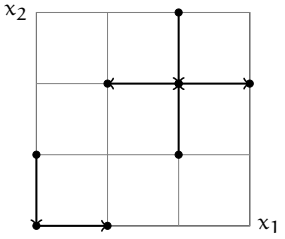

Figure 13: Visual example of trajectories in the Morris method, with a step-by-step description of the Morris method's principles for a model with 2 input factors.

Gash model for interception instead of the Von Hoyningen-Hüne and Braden model (increasing the number of factors to 34).

For the chosen maximum perturbations of -15% and +15% around the arithmetic mean, the corresponding percentiles for topsoil θ_s are the 6^{th} and 94^{th} using a fitted normal distribution. For topsoil K_s, -15% and +15% correspond to the 52^{th} and 69^{th} percentile (using a non-symmetric lognormal distribution). A maximum perturbation of 15% is then a large underestimation of the occuring variability in K_s. Therefore, another Morris experiment has been done with a larger range for K_s, also between its 6^{th} and 94^{th} percentile (15.5 and 169.5 cm d^{-1} respectively).

2.5.2 *Simulation of recharge*

The study area was divided into four simulation units, one for each vegetation type (the ranking of factors in the sensitivity analysis suggest this is appropriate, as vegetation characteristics are relatively important.)
These simulation units differ only from each in other with respect to vegetation characteristics, such as rooting density, vegetative soil cover, and crop factors. The Gash model for closed canopies for interception was used for the forest simulation unit, the Von Hoyingen-Hune and Braden model for the other simulation units. The area of these simulation units is shown in table 2. Average groundwater recharge (in m^3 y^{-1}) has been calculated by multiplying the drainage as calculated by SWAP for a simulation unit, by the corresponding area for that simulation unit.

Table 2: Simulation unit area.

Land cover	Area (m^2)	% of total
Shrubland	5211167	57.7
Forest	2382745	26.4
Pasture	898578	10.0
Airport	343349	3.8
Roof	191661	2.1
Total	9027501	100

Three scenarios for rainfall were used: average yearly rainfall sums of 980 mm (St. Kitts), 1089 mm (Braak, 1935), and 1304 mm (Taylor and Works). St. Kitts is the only long term rainfall timeseries with a daily resolution and has therefore been used to distribute the rainfall in time: the 1089 mm and 1304 mm timeseries were generated by increasing the precipitation of St. Kitts at all times in the simulation period (times 1.11 for 1089 mm and times 1.33 for 1304 mm).

Roofs in the study area call for a separate treatment: water falling on roofs does not infiltrate – at least not directly. Many of the buildings have cisterns to store rainwater. This rainwater is then used for drinking, washing, and so forth, and ends up in cesspits. The assumption made here is that all water that falls on roofs eventually ends up in cesspits and infiltrates as sewage water from there. To determine

Table 3: Sensitivity analysis model input factors. Rainfall, duration of rainfall, and reference evapotranspiration have no single baseline value since they vary in time; the perturbation was applied at all times in the study period. Due to discretization, soil depth varies slightly differently, and has four actual levels of 50, 55, 60, and 65 cm. Parameters noted with * were used only in the first sensitivity analysis, parameters noted with ** were used only in the second sensitivity analysis (in which the Gash model for interception was used instead of the Von-Hoyingen-Hüne and Braden model).

Input	Description	Baseline value
Rain	Rainfall	-
Wet	Duration of rainfall	-
ETref	Reference evapotranspiration	-
CFBS	Soil evaporation factor	1.0
COFRED	Soil evaporation coefficient of Black	0.35
layer1depth	Depth of topsoil layer	60.0 cm
ORES1	Topsoil residual soil moisture content θ_r	0.140 cm^3 cm^{-3}
OSAT1	Topsoil saturated soil moisture content θ_s	0.516 cm^3 cm^{-3}
ALFA1	Topsoil Van Genuchten's α	0.0283 cm^{-1}
NPAR1	Topsoil Van Genuchten's n	1.426
KSAT1	Topsoil saturated hydraulic conductivity K_s	78.4 cm d^{-1}
LEXP1	Topsoil Van Genuchten's λ	0.5
ORES2	Subsoil residual soil moisture content θ_r	0.04 cm^3 cm^{-3}
OSAT2	Subsoil saturated soil moisture content θ_s	0.41 cm^3 cm^{-3}
ALFA2	Subsoil Van Genuchten's α	0.038 cm^{-1}
NPAR2	Subsoil Van Genuchten's n	2.474
KSAT2	Subsoil saturated hydraulic conductivity K_s	823 cm d^{-1}
LEXP2	Subsoil Van Genuchten's λ	0.5
GCTB	Vegetative soil cover	0.81
CF	Crop factor	1.05
RD	Rooting depth	78.0 cm
HLIM1	Root water extraction parameter	-10 cm
HLIM2U	Root water extraction parameter	-25 cm
HLIM2L	Root water extraction parameter	-25 cm
HLIM3H	Root water extraction parameter	-200 cm
HLIM3L	Root water extraction parameter	-200 cm
HLIM4	Root water extraction parameter	-800 cm
ADCRH	Level of high atmospheric demand	0.5 cm d^{-1}
ADCRL	Level of low atmospheric demand	0.1 cm d^{-1}
COFAB*	Interception coefficient	0.25 mm
PFREE**	Free throughfall coefficient	0.5
SCANOPY**	Canopy storage	0.4 mm
AVPREC**	Average precipitation intensity	18 mm d^{-1}
AVEVAP**	Average evaporation intensity during rainfall	2.5 mm d^{-1}

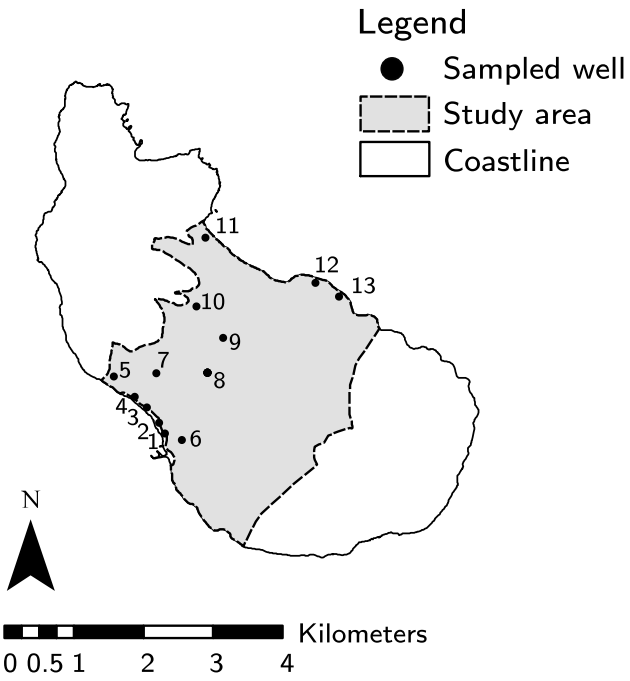

Figure 14: Locations of sampled wells.

this quantity, the amount of roofed area in the study area has been determined in ArcGIS (ESRI, 2011) from a satellite image from Bing maps Bing Maps (2014) and this area has been multiplied by the rainfall in the study period.

2.6 GROUNDWATER

Groundwater samples have been taken from 13 wells in 2014 and chemically analzyed for nitrate, nitrite, ammonium, and phosphate (personal communication I. Firmansyah). See figure 14 for the location of the wells. Four Schlumberger Diver Loggers were installed to measure groundwater levels over a period of nine months in 2014, from May 2014 to January 2015 in wells 3, 8, 9, and 13. A fifth Diver was kept on the island to measure atmospheric pressure.

3

RESULTS AND DISCUSSION

3.1 RAINFALL AND METEOROLOGY

The availability of meteorological data is not ideal. The quality of the data from the airport of St. Eustatius were deemed to poor to use, so that the records from the measurements at the airport of St. Kitts were used instead. Average yearly rainfall amounts to 980 mm $year^{-1}$ for the airport of St. Kitts for the period 1983–2013, 1304 mm $year^{-1}$ for the measurements of Taylor and Works for the period 1984–2013, and 1089 mm $year^{-1}$ for the period 1881–1933 Braak (1935). The range of estimated yearly average rainfall is thus quite large.

However, uncertainty regarding spatial variability over St Eustatius remains. One can imagine that while the Quill is a relatively small topographic feature, it could locally affect rainfall. Rojer (1997) claims the Quill arrests clouds, causing more rainfall than on the plains. Braak (1935) features rainfall data measured at stations at a heights up to 300 meters a.s.l. but no orographic effect on rainfall is visible. Based on Braak (1935), Augustinus et al. (1985) conclude that "Maybe the island is too small to produce differences due to exposure anyway", although the number of years measured for some locations, six, is not large. Smith et al. (2009a) and Smith et al. (2009b) investigated orographic effects on Dominica and conclude orography affects rainfall strongly. However, Dominica is much larger than St. Eustatius and has much higher peaks (up to 1447 m a.s.l.). Sobel et al. (2011) conclude that enhancements of rainfall or rainfall frequency for small islands are statistically insignificant. Regardless, estimating the strength of the orographic effect without quantitive rainfall data is unfeasible. Rainfall was therefore assumed to be uniform.

Other meteorological variables will also vary in space. The Quill will shade parts of the study area, although shading is limited due to proximity to the equator. Wind generally decreases passing over land, encountering aerodynamic roughness, but St. Eustatius's land surface is small – but again, without measurements distributed over the island wind is assumed to uniform.

With regards to available moisture, it is also possible that any eventual windward orographic effects on rainfall are compensated for by greater evapotranspiration, caused by higher wind speeds. The north eastern (windward) part of the island appears to be drier. During the field work period, the shrubs on the north eastern part of the island generally had much less dense canopies than those in more and central and western sites; the fraction of dead shrubs was greater, the

shrubs possibly having been killed off by the foregoing (severe) dry season. Lack of soil water retention could also have played a role, but the dead shrubs were found on the eastern part of the island, showing no correlation with soil strata as identified by Veenenbos (1955).

Suitability St. Kitts data

Table 4 shows means and standard deviations for both meteorological stations and R^2 between the daily observations. Despite a distance of only 35 km, measured values at St. Eustatius and St. Kitts differ notably. R^2 is poor for all variables, and in particular for diurnal temperature range. Assuming temperature range is a good proxy for solar radiation and cloud cover, clouds may be especially local, covering one airport but not the other.

Table 4: Comparison of daily meteorological variables. μ and σ are mean and standard deviation, respectively.

Meteorological variable	Measure	St. Eustatius	St. Kitts
Temperature (°C)	μ	27.8	27.3
	σ	1.59	1.41
	R^2	0.509	
Diurnal temperature range (°C)	μ	5.12	6.18
	σ	1.58	1.29
	R^2	-0.720	
Relative humidity (%)	μ	73.9	76.1
	σ	7.67	5.52
	R^2	0.146	
Wind speed (m s^{-1})	μ	5.35	5.36
	σ	1.85	1.69
	R^2	0.471	

Fortunately, for the purposes of this study, agreement in day-to-day weather is not very important. St. Eustatius measures higher temperatures, but a lower diurnal temperature range. St. Eustatius also appears to feature lower relative humidities. These differences are not easily explained by the locations of the stations on the islands. They could also be due to systematic measurement errors. Table 4 shows means agreeing relatively well, although overestimation on St. Kitts or underestimation on St. Eustatius of diurnal temperature range is suggested. Monthly rainfall sums also agree poorly, with an R^2 of 0.216, again underscoring that even on monthly timescales, the weather of St. Kitts is not the weather of St. Eustatius. We can see in figure 15 that monthly rainfall sums doUs have similar distributions, but distressingly, the mean monthly rainfall is much higher for St. Eustatius: 109 mm versus 81 mm. The difference in rainfall over a 30

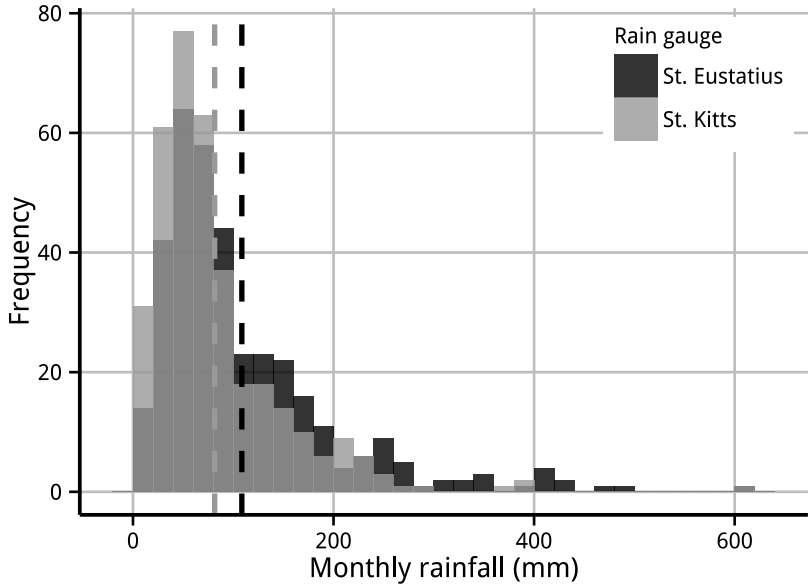

Figure 15: Histogram of monthly rainfall for St. Eustatius and St. Kitts in the period 01-01-1983 to 31-12-2013.

year period amounts to 25% – and the 8% missing values for St. Kitts cannot explain this discrepancy alone. Assuming 8% of the rain in St. Kitts has gone unrecorded, the 'true' average yearly rainfall can be calculated by multiplying 980 mm by $\frac{100}{92}$. This results in a value of 1065 mm, which is similar to the average of 1098 mm found by Braak (1935). In terms of yearly rainfall sums, St. Kitts airport data has the lowest sum at 980 mm, the Works' dataset the highest at 1304 mm, and Braak (1935) in between at 1089 mm. In conclusion, orography could play a role, since the rain gauges of Taylor and Works were located at an elevation of 175 m a.s.l., while St. Kitts airport is located at 52 m a.s.l and Braak (1935) reports an elevation of 49 m a.s.l. As mentioned earlier, however, this hypothesis remains untested.

For the SWAP simulations, three scenarios have been investigated: with yearly rainfall sums of 980, 1089, and 1304 mm. In every scenario, the St. Kitts data has been used as the 'template': annual rainfall of e.g. 1304 mm was simulated by multiplying all rainfall values in the St. Kitts dataset by (1304/980 =) 1.33.

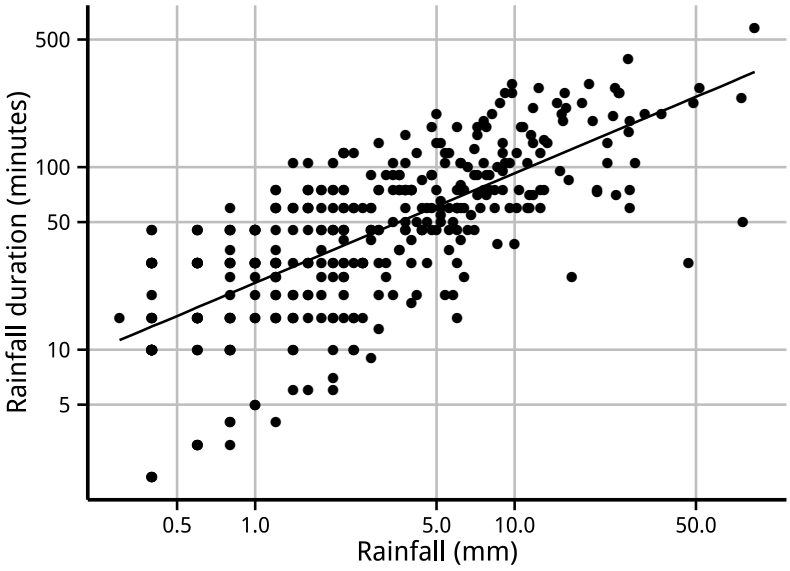

Figure 16: Relation between rainfall P and rainfall duration t_{rain} for 403 rainfall events with indication of the regression line $t_{rain} = \exp(0.60 \ln(P) + 3.15)$. R^2 = 0.53

Rainfall duration

The relationship between daily values of rainfall and rainfall duration was found to be described best by

$$t_{rain} = \exp(0.60 \ln(P) + 3.15) \tag{16}$$

where t_{rain} (minutes) is rainfall duration, and P (mm) is rainfall per day. See also figure 16. Cross validating this model 1000 times gives an average R^2 of 0.53, with a standard deviation of 0.093. The chosen relationship covers the entire range of precipitation sums well, predicting a rainfall duration of 10 minutes for the minimum recorded precipitation of 0.25 mm and a duration of 560 minutes (9 hours) for the maximum sum of 200 mm. For the median rainfall of 2.3 mm, a duration of 38 minutes is predicted. While the predicted rainfall duration is not very accurate and based only on a short timeseries of two years, the resulting rainfall intensities are more comparable to measured intensities than the intensities that result from applying rainfall over the entire day.

Using this method to determine rainfall duration for SWAP appears to have negligible effects when compared to measured rainfall durations: drainage for the test year 2013 is 44.6 mm for 15 minute rainfall data versus 44.9 mm for aggregated data.

Table 5: Statistical performance in cross validation of the various radiation estimation models for the period 13-01-2013 to 13-01-2015. MBE is mean bias error and MAE is mean absolute error. $\overline{\text{MBE}}$, $\overline{\text{MAE}}$ and $\overline{R^2_{adj}}$ are average MAE, MBE, and R^2_{adj} of the cross validation. For comparison, mean daily solar radiation amounts to 16.4 MJ d^{-1}.

Model	Equation	$\overline{\text{MAE}}$ (MJ d^{-1})	$\overline{\text{MBE}}$ (MJ d^{-1})	$\overline{R^2_{adj}}$ (-)
H	$R_s = K_{Rs}\sqrt{\Delta T}R_a$	3.1	-1.0E-1	0.30
BC	$R_s = T_{t,max}(1-\exp(-C_1\ \Delta T^{C_2}))R_a$	3.0	-1.8E-1	0.33
M1	$R_s = (K_{Rs}\sqrt{\Delta T})R_a + K_1$	3.0	-1.3E-2	0.31
M2	$R_s = (K_{Rs}\sqrt{\Delta T} - K_1 RH + K_2)R_a$	2.7	-1.7E-1	0.46
M3	$R_s = (K_{Rs}\sqrt{\Delta T} - K_1 RH + K_2)R_a + K_3$	2.4	5.9E-4	0.55
M4	$R_s = (K_{Rs}\sqrt{\Delta T} - K_1 RH + K_2\ T + K_3)R_a + K_4$	2.3	1.1E-3	0.58
M5	$R_s = (K_{Rs}\sqrt{\Delta T} - K_1 RH + K_2 W + K_3)R_a + K_4$	2.3	-1.4E-3	0.56

3.2 REFERENCE EVAPOTRANSPIRATION

Solar radiation

Table 5 shows the results of the cross validation of the various radiation models. The unmodified Hargreaves (H) and Bristow-Campbell (BC) models perform similarly, both underestimating daily solar radiation on average ($\overline{\text{MBE}}$), and with a rather poor fit ($\overline{\text{MAE}}$ and $\overline{R^2_{adj}}$). It is clear that the inclusion of relative humidity (model M2 and M3) strongly increases the performance of the solar radiation estimation. In contrast, the inclusion of temperature (M4) or a switch for wet days (M5) has relatively little effect, both in terms of MAE (mean absolute error) and R^2_{adj}. Based on the only slight increases in $\overline{\text{MAE}}$ and $\overline{R^2_{adj}}$, M4 and M5 have been discarded. With an R^2_{adj} of 0.55, the accuracy of M3 is still not very good. Regardless, the real test is whether this method outperforms that Hargreaves-Samani method: the reference evapotranspiration estimate that resembles the FAO Penman-Monteith method with measured solar radiation the most, is the better model.

In terms of alternative radiation models, several researchers have elaborated the Bristow-Campbell model. Thornton and Running (1999) refined the methods for estimating maximum transmissivity $T_{t,max}$, and the two emperical coefficients C_1 and C_2. They added a correction for water vapor pressure in $T_{t,max}$, a minimum value for transmittance, and added another empirical coefficient. However, this method could not be applied for St. Eustatius. The set of equations was not calibrated for the climate: the used dataset featured only a single station, Miami, in a tropical climate. The method performed especially poorly at estimating solar radiation at Miami. Additionally, the

method could not be realistically calibrated for local conditions in St. Eustatius because of data requirements. The same is true for the modified Bristow-Campbell models in Donatelli and Campbell (1998) and Donatelli and Bellocchi (2001). Both of these models are more complex than the Bristow-Campbell model, which makes it difficult to elaborate and callibrate them.

The models based on the Hargreaves radiation formula are not suitable for extrapolation: it will probably not estimate radiation accurately when the input values exceed the range observed in the the two years. For example, a particularly large temperature range ΔT can result in solar radiation R_s exceeding extraterrestrial radiation R_a (the Bristow-Campbell model performs better in this regard). To avoid this issue, values that were outside of the two year observational range were replaced with the boundary values, for the final purpose of estimating solar radiation for the study period.

Options for reference evapotranspiration

Table 6 shows the results of the cross validation of the FAO Penman-Monteith method with solar radiation estimated using M3, hereafter called the reduced FAO method, and the Hargreaves-Samani method. The reduced FAO method is much closer to the 'true' reference evapotranspiration, as estimated by the FAO Penman-Monteith method with measured solar radiation, than the Hargreaves-Samani method. The reason is obvious: all inputs except solar radation are the same; the reduced FAO method is a better method because it can incorporate more relevant data.

Table 6: Statistical performance in cross validation of the Hargreaves-Samani method and the FAO Penman-Monteith method with estimated solar radiation, versus the FAO Penman-Monteith method with measured solar radiation. The analyzed period is 13-01-2013 to 13-01-2015, using data from the Works' weather station. $\overline{MBE}$, $\overline{MAE}$ and $\overline{R^2}$ are average MAE, MBE, and R^2 of the cross validation, with standard deviations included. For comparison, average daily reference evapotranspiration amounts to 3.44 mm d^{-1}.

Method	$\overline{MAE}$ (mm d^{-1})	$\overline{MBE}$ (mm d^{-1})	$\overline{R^2}$ (-)
Hargreaves-Samani	0.61±0.014	-0.39±0.022	0.21±0.043
Reduced FAO-PM	0.36±0.011	-0.0044±0.034	0.68±0.021

However, the low data requirements of the Hargreaves-Samani method are also an advantage. Humidity is difficult to measure accurately without modern equipment and the accuracy of wind speed measurements are not easy to assess (Droogers and Allen, 2002). Temperature, in comparison, is easy to measure. Indeed, the accuracy of

the meteorological data from the airport of St. Kitts is not easily assessed.

Troubling about the Hargreaves-Samani method here is its apparent 11% underestimation of reference evapotranspiration, and this is particularly troubling behaviour given the purpose of estimating groundwater recharge. In fact, underestimation will be more severe when we take into account the location of the Works' weather station. It measures much lower wind speeds than the meteorological station at the airport due to a sheltered location, while most of the study area will be subject to these high wind speeds. Higher wind speeds will result in more evapotranspiration, and wind speed is not an input of the Hargreaves-Samani method. In conclusion, the reduced FAO method appears much more appropriate than the Hargreaves-Samani method for estimating reference evapotranspiration on St. Eustatius – with the assumption that the meteorological data from St. Kitts is reliable.

Evapotranspiration estimates agree with those found from meteorological stations on Puerto Rico (Harmsen, 2003), who found an average evapotranspiration of 3.3–4.1 mm d^{-1} using the FAO-56 Penman-Monteith equation. The Penman-Monteith method is a robust tool for estimating evapotranspiration, but its reliability is primarily influenced by canopy resistance parameterization (see the following section) and solar radiation (Langensiepen et al., 2009) – both of which have not been measured for the study period, but estimated. This means evapotranspiration is an important source of uncertainty in the estimate of groundwater recharge, but lack of data on the errors on the variables means that its effects cannot be quantified yet.

3.3 VEGETATION

It proved difficult to characterize the vegetation in the study area accurately. Firstly, there is the challenge of describing vegetation on the scale of the study area without the aid of vegetation remote sensing data. Secondly, there is variability in time. For example, on long timescales vegetation sprouts, grows and finally dies; on shorter timescales plants may shed their leaves. FAO-56 explicitly accounts for this by normally using three crop factors: one for the beginning, mid, and the end of the growing season. Anthropogenic influences too play an important role. Areas are cleared of shrubs, or areas previously maintained may become abandoned. Plots may become fenced to keep in or keep out cattle, changing grazing intensity. This can greatly affect the generation of groundwater recharge (Scanlon et al., 2005). None of this dynamic behaviour has been measured or simulated given the scope of the research.

Furthermore, vegetation was recorded only once, in December, at what is generally the end of the wet season. Without a measuring campaign that spans several years, the representativity of these measurements is difficult to gauge. The vegetation on average could both be more or less lush: I arrived at the beginning of the wet season, and the foregoing months had been exceptionally dry, even for a dry season. Without additional measurements, I am forced to assume that the measured vegetation state is representative for the study period – this assumption is highly uncertain.

It is particularly challenging to simulate the evapotranspiration of the vegetated areas in the built-up class. It is very uncertain how well the vegetation in these areas actually resembles that of the shrubland. Buildings could strongly affect the micrometeorological conditions, e.g. by funneling winds or by shading vegetation; modified land surfaces heat up more strongly, also affecting micrometeorological conditions. Additionally, residents might also irrigate their gardens.

Crop factors

The results of the fieldwork for vegetative soil cover and vegetation height can be found in table 7. The values have been averaged into a single value for a class across all the landscape units that feature that class. In reality, the shrubs may differ per landscape unit, depending on location. For example, shrubs on the windward side may have less dense canopies; average canopy cover for the eastern part was 0.46, versus an average 0.58 for the entire study area. However, given the small number of measurements at one only one point in time in this research, such heterogeneities could not be investigated in detail, so that a study area-wide average has been used instead.

Table 7: Vegetation data. h is averaged maximum vegetation height, f_c is averaged vegetative soil cover, N is the number of samples, r_l is the crop mean leaf restistance taken from Descheemaeker et al. (2011), F_r is the calculated stomatal control resistance factor, and K_{cb} is the calculated basal crop coefficient.

Vegetation type	h (m)	f_c (m^2 m^{-2})	N (-)	r_l (s m^{-1})	F_r (-)	K_{cb} (-)
Pasture grass	0.06	0.91	47	133	0.91	0.92
Shrubland grass	0.49	0.88	50	133	0.97	0.95
Shrubland shrubs	2.8	0.58	56	202	0.76	0.83
Forest	7	0.73	36	245	0.69	0.83

Due to lack of special equipment a part of the photos were likely taken at a slight angle instead of straight up (I estimate an error of circa 10 degrees). This would then result in an overestimation of vegetative cover. Further, estimating vegetative soil cover visually is highly subjective. We may thus assume estimated vegetative soil covers are uncertain, but not inappropriately so considering the use in the FAO-56 method for estimating crop coefficients. After all, this method strongly simplifies vegetation, describing it only in terms of vegetative soil cover, average maximum vegetation heigth, and a stomatal resistance.

The r_l values in table 7 have been measured in Ethiopia, with comparable land use. Although both climates are semi-arid, St. Eustatius has a maritime climate, while the measurement site in Ethiopa has a continental climate. Allen et al. (1996) gives resistances for many canopy types and the values found show some agreement, but also show that values in literature can vary wildly for a single canopy type. Uncertainty regarding the stomatal control factor thus remains high.

Basal crop coefficients K_{cb} estimated with the FAO-56 method can be found in table 7. Despite differences in vegetation height h and vegetative soil cover SC between forest and shrubs, the FAO-56 method for determing the basal crop coefficient K_{cb} results in the same values due to the compensating effect of the stomatal control factor F_r. This factor has been calculated from r_l, which was not measured in the study area but has been taken from Descheemaeker et al. (2011). Table 8 shows the crop factor used in SWAP.

Table 8: SWAP crop factors.

Land cover class	K_{cf}	SC
Pasture	1.01	0.91
Airport	1.00	1.00
Shrubland	1.05	0.81
Forest	1.06	0.81

One may call into question the suitability of the FAO-56 procedure for *daily* calculation of evapotranspiration for forest or shrub vegetation, where first a reference evapotranspiration ET_{ref} is calculated and then translated to the crop using a crop coefficient K_{cb}. Aerody-

namic resistance is in general an order of magnitude smaller for forest than for grassland. Consequently, forest evapotranspiration will be much more sensitive to changes in stomatal resistance (Kelliher et al., 1993). A constant crop factor cannot simulate this sensitivity.

Spatial scaling also poses a challenge. When faced with a part of the landscape of which we have measured of invidiual plants average maximum vegetation heights h and vegetative soil cover SC, how do we average h and SC so that the method used here for estimating a crop factor provides a crop factor that is representative for that part of the landscape? I have used the arithmetic mean, but other means might be more appropriate for this method of estimating crop factors due to e.g. clothesline effects on evapotranspiration; FAO-56 provides equations for intercropping of multiple crops in this context, but does not comment on heterogeneity within a type of crop.

There is an alternative option available in SWAP to calculate evapotranspiration more dynamically with the Penman-Monteith equation directly, but this requires more data: on stomatal and aerodynamic resistances, on the height of the vegetation, and the albedo. SWAP also has the option of using leaf area index (LAI) instead of vegetative soil cover. However, leaf area index is more difficult to determine than soil cover, as it cannot be easily visually determined in the field. Applying these options for further research would likely give more reliable results but would also require less simple methods for recording vegetation.

However, in case of multi-component canopies, there is the problem of determining inner canopy resistances (Lhomme et al., 2013). In comparison, crop factors are much simpler to work with, relatively robust, and available for many vegetation types – albeit almost exclusively agricultural crops. In terms of estimating crop factors, however, there appears to exist very little scientific hydrologic literature. Any alternative method will very likely require variables that are difficult or time consuming to measure, such light and water use efficiencies, or leaf and aerodynamic resistances. Additionally, even when these variables have been measured, they generally have to be upscaled to field or landscape scales. The biggest advantage of the FAO-56 method is that it has some confirmation in field experiments, but crop coefficients estimated with this method will be uncertain, even with highly certain vegetation data. Its adequacy does not appear to have been solidly established. Only two applications can be found in literature: Ringersma and Sikking (2001) and Descheemaeker et al. (2011) found representative estimates in (semi-)arid climates, although Ringersma and Sikking (2001) reported an overestimating of the crop coefficient when using leaf area index in the method.

Rooting depth

Figure 17 shows the schematized rootzone distribution used in SWAP. Because a thorough investigation of root distributions in the study area was outside of the scope of this research, these root density distributions are rather uncertain. Especially those for shrubland and forest are uncertain, since they have not actually been observed. While the distributions taken from the dataset should reflect the climate well, soil properties and specific plant physiology may not be reflected well. Furthermore, many of the depths in the dataset of (Schenk and Jackson, 2002) were in fact extrapolated depths — the individual investigations often did not unearth root systems in their entirety.

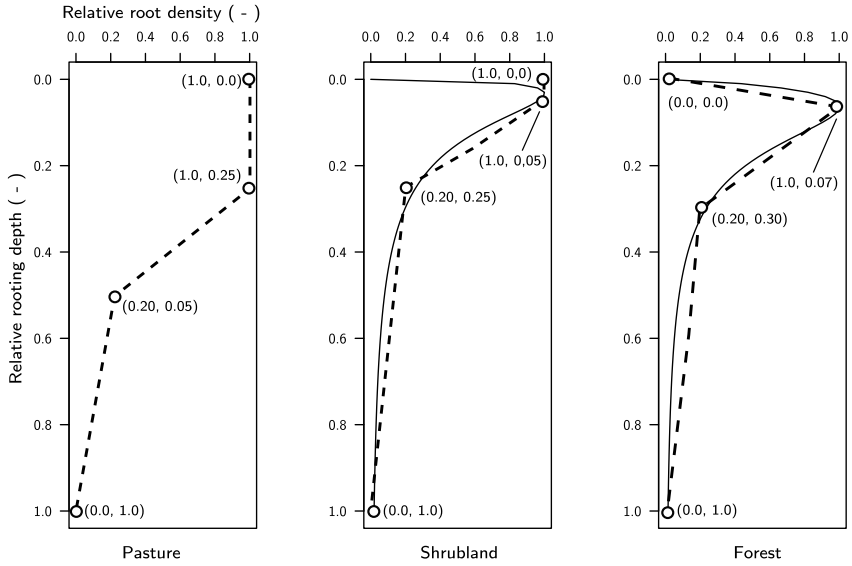

Figure 17: Root density distributions for land cover classes. Solid lines for shrubland and forest are distributions taken from Schenk and Jackson (2002) calculated with equation (7). Dashed lines are schematized root density distributions, with the graph coordinates used as model input. The pasture root density distrubtion was estimated in the field, with a maximum depth of 0.60 m. For shrubland c_r, maximum depth (D95), and D50 of -1.336, 0.78 m, and 0.11 m respectively were found; for forest, -1.681, 0.83, and 0.12.

3.4 SOIL HYDRAULIC PROPERTIES

Field work

Based on four observations in the field, see figure 18, the soil was schematized into two layers for simulation: a sandy loam layer (dark brown) on top and gravelly sand layer (orange and light grey) for the rest of the soil column. From these observations, the orange material appears different in colour but not in structure from the deeper material: it is all very coarse sand and gravel, so that identical hydraulic properties have been assumed. A thickness of 60 cm was estimated for the sandy loam layer. This is within the range of the observations of Roobol and Smith (2004), who report that the entire study area is covered by a deposit varying in thickness between 30 and 110 cm, with a median value of 55 cm (based on 21 stratigraphic sections). The gravelly sandy layer was assumed to span from a depth of 60 cm to the end of the simulated soil column, at 300 cm.

The gravelly sand layer could not be investigated much since it is covered by the sandy loam layer nearly everywhere. Only five soil samples and three conductivity measurements have been taken of this layer. Only one location was available for sampling and measurement and the gravelly nature of the soil made both sampling and measuring conductivity very challenging. The soil surveys done in the past also almost exclusively describe the sandy loam layer, so data is very scarce on the material underneath it. Based on the analysis of Roobol and Smith (2004) and observations in the field, it seems that coarse sediments underlie the sandy loam layer everywhere in the study area. The sandy loam layer is the layer in which the vegetation roots, from which soil moisture is taken up, and therefore defining for groundwater recharge. For these reasons, the following discussion focuses on the observations of the sandy loam layer.

Heterogeneity is not clearly detectable in the measurements of θ_S and K_s of the sandy loam layer, and the number of measurements is too small to make a distinction between the soil strata as identified by Veenenbos (1955). Veenenbos (1955) and Augustinus et al. (1985) report a high degree of stoniness for the upper parts of the Quill. K_s and θ_s can be adjusted using the method of e.g. Hlaváčiková and Novák (2014), but again there is simply not enough data available to make reliable estimates of the effects of stoniness on K_s and θ_s. No significant difference was found between surface and subsurface in terms of saturated water content or saturated hydraulic conductivity of the sandy loam layer ($p=0.78$ and $p=0.72$, respectively, for Wilcoxon rank sum test). A homogeneous soil has therefore been assumed for the entire study area, and the additional 46 hydraulic conductivities measured by Wouter (Ten Harkel, 2015) are included in the analysis.

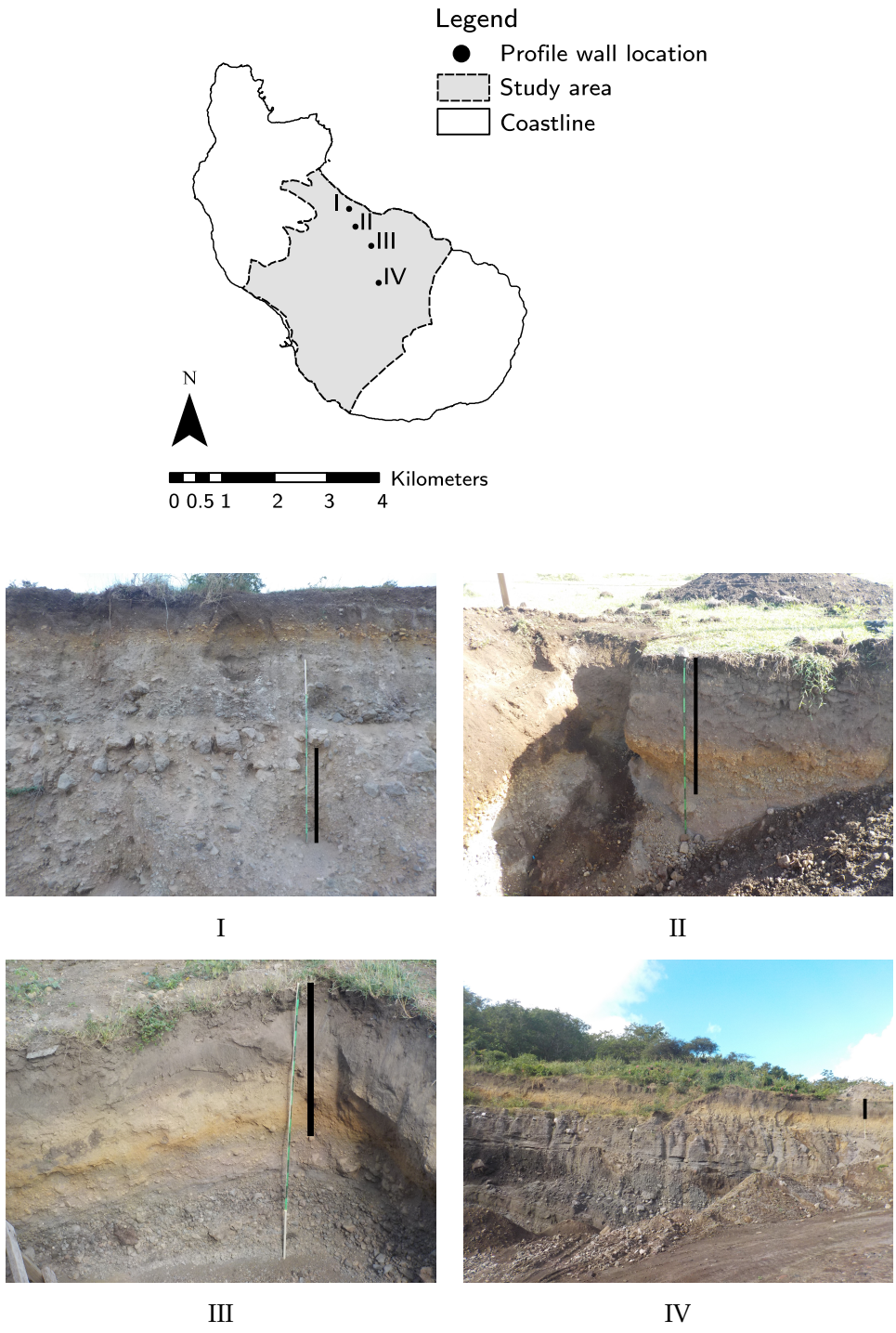

Figure 18: Four soil profiles in the study area. The black lines indicate a length of 1 m for scale.

The distribution of measured saturated water content is shown in figure 19. Saturated water content is relatively high, with a mean value of 0.51 cm^3 cm^{-3}. The soil samples may have suffered some compaction from hammering the sampling rings into the soil and some air might have been trapped in the samples during saturation. Calculating average porosity from measured bulk densities and an assumed mineral density of 2.65 g cm^{-3} results in a value of 0.58 ^{3} cm^{-3}, suggesting incomplete saturation. However, air is encapsulated in field conditions as well (Fayer and Hillel, 1986) so that the value of 0.51 cm^3 cm^{-3} has been used as θ_s in modeling.

Figure 20 shows the distribution of measured saturated hydraulic conductivities. Saturated conductivity varies greatly, ranging from 6 cm d^{-1} to 320 cm d^{-1}. While some uncertainty exists in terms of using disk infiltrometers and its analysis using the method of Zhang (1997) (Vandervaere et al., 2000), a much larger uncertainty (in terms of modeling groundwater recharge) is caused by upscaling small soil hydraulic property measurements for large-scale modeling (Hopmans et al., 2002). Generally, there does not exist a set of effective parameter values for a large scale unit: average soil parameters do not necessarily result in average soil water flow (Philip, 1980). Regardless, the arithmetic mean has been used for both K_s and θ_s in modeling; as will be shown, the results of the sensitivity analysis justify this simplification.

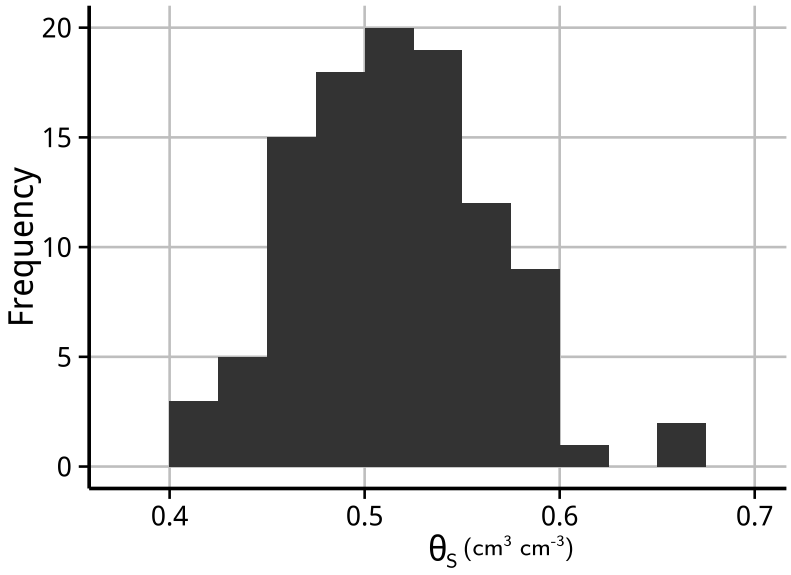

Figure 19: Histogram of measured saturated water contents.

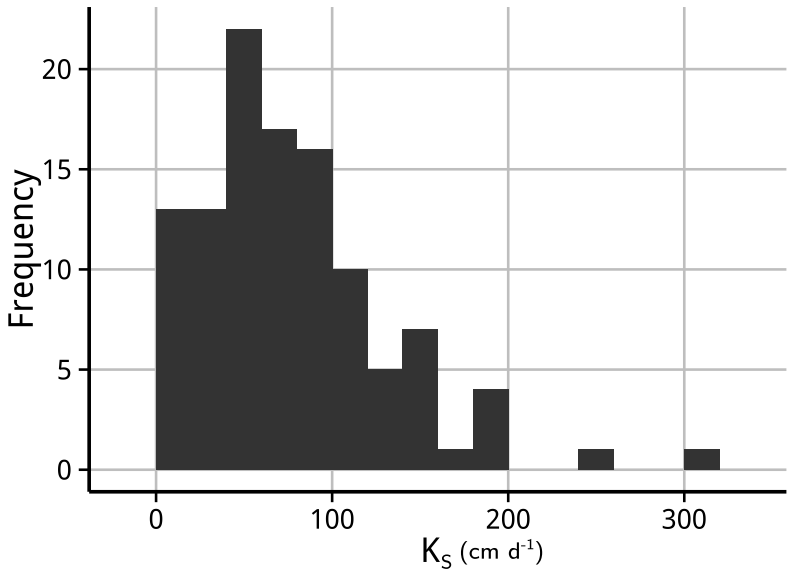

Figure 20: Histogram of measured saturated hydraulic conductivities.

Pedotransfer function

The soil hydraulic parameter values generated with the pedotransfer function are shown in table 9. With little quantitative data available, uncertainty is again difficult to assess. Veenenbos (1955) and Augustinus et al. (1985) analyzed a small number of relevant samples, so the input of the pedotransfer function may not be representative (especially for the bottom layer). Another uncertainty is caused by pedotransfer function structure; confidence intervals such as provided by the pedotransfer function model Rosetta (Schaap et al., 2001) greatly benefit uncertainty analysis, but are not provided by Hodnett and Tomasella (2002). The predicted average θ_s of 0.49 cm^3 cm^{-3} agrees well with the average measured value of 0.51, which suggests the pedotransfer function is appropriate for this soil. Pedotransfer functions for temperate soils give much lower values in comparison: Rosetta (Schaap et al., 2001) predicted a saturated water content of 0.37 for the topsoil in the study area. This underscores the importance of pedotransfer functions specific to tropical soils (Hodnett and Tomasella, 2002).

Table 9: Soil hydraulic parameters for SWAP. θ_r, α, and n have been determined using a pedotransfer function. The sandy loam layer (layer 1) has a depth of 60 cm, the rest of the 300 cm deep column consists of the gravelly sand (layer 2).

Layer	θ_r (cm^3 cm^{-3})	θ_s (cm^3 cm^{-3})	α (cm^{-1})	n (-)	K_s (cm d^{-1})	λ (-)
1	0.14	0.516	0.0283	1.426	78.4	0.5
2	0.04	0.410	0.0384	2.474	823.0	0.5

3.5 SWAP SIMULATION

3.5.1 *Sensitivity analysis*

The results of the Morris experiments are displayed in figure 21, 22, and 23. μ^* can be used to rank the parameters in order of importance for determining groundwater recharge, but this ranking might vary somewhat between Morris experiments due to the limited random sampling of the input space (with $p = 4$ levels and $k = 31$ factors, there are $31^4 = 923521$ possible points for the trajectories to pass through). Ranking groups of parameters is therefore more appropriate than ranking invidual parameters based on small differences in μ^*. Theoretically, reference evapotranspiration (ET) and crop factor (CF) should be almost the same in terms of μ^* and σ: potential transpiration is a product of these, so that on average the results of a peturbation in (ET) should be very similar to the results of the same peturbation in CF. ET affects both plant transpiration and soil evaporation, whereas CF affects only transpiration, but evaporation is small compared to transpiration. I hypothesize that the differing results must be mainly due to the limited random sampling of the input space; indeed figure 23 shows them closer together. With a larger number of trajectories r, the results for ET and CF should lie closer together. The findings of Ruano et al. (2012) support this hypothesis, who found that the number of 10–20 trajectories recommended by Campolongo et al. (2007) may be too small.

The boundary conditions, rainfall and potential evapotranspiration (product of crop factor and reference evapotranspiration), are clearly the most important in determining recharge. Fortunately, groundwater recharge is not especially sensitive to any of the factors that were especially difficult to determine or were left at SWAP default values – e.g. rooting depth, interception parameters, or soil water water extraction parameters.

Comparing figure 21 with figure 22 shows that a ranking based om μ would have given almost the same results. All of the important factors are monotonous, except for the topsoil Van Genuchten's n (NPAR1). The points lie around the diagonal in figure 21; generally, factors with a high μ^* also have a high value for σ. None of the factors have a purely linear effect on recharge. Based on this sensitivity analysis – depending somewhat on the chosen cutoff for μ^* – up to 21 factors could be fixed when SWAP is used to produce groundwater recharge estimations. In overview, rainfall and factors involved with potential evapotranspiration are the most important (reference evapotranspiration, crop factor, vegetative soil cover (GCTB)). Some properties of the top layer are next in importance, but interestingly, K_s is not one of the important properties of the top layer. The sensitivity analysis with a larger range in K_s did not result in appreciable

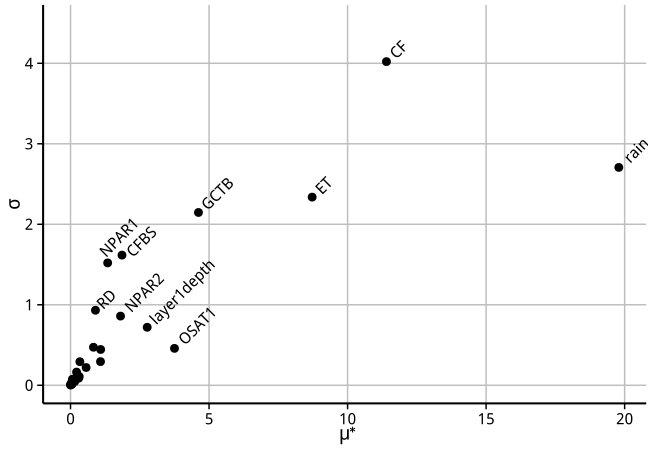

Figure 21: Morris sensitivity measures μ^* and σ for 31 input factors, all deviating up to 15% from their baseline values. Only the most important factors are labelled. See table 3 for label descriptions.

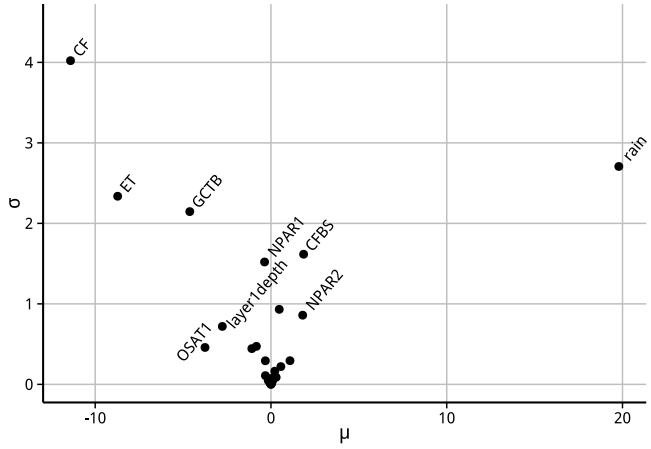

Figure 22: Morris sensitivity measures μ and σ for 31 input factors, all deviating up to 15% from their baseline values. See table 3 for label descriptions.

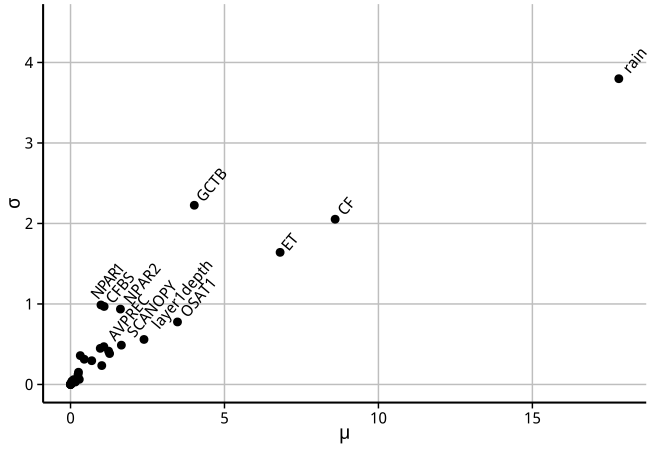

Figure 23: Morris sensitivity measures μ^* and σ for 34 input factors using the Gash model for interception, all deviating up to 15% from their baseline values. See table 3 for label descriptions.

differences: μ^* for K_s did increase but was still small. Long term average groundwater recharge simply does not appear to be sensitive to K_s. K_s appears to be high enough that water is not retarded much.

Using the Gash model for interception does not change the picture a great deal (figure 23): the first six most important parameters are the same. Interception does play a larger role, as two Gash model parameter become recognizable (canopy storage (SCANOPY) and average precipitation rate (AVPREC)).

Note that an increase in the soil evaporation factor (CFBS) leads to higher recharge – CFBS only plays a (somewhat nonintuitive) role in distributing potential evapotranspiration between potential transpiration and potential evaporation; it cannot actually increase evapotranspiration. So, potential transpiration is decreased, and this decrease is not compensated for by higher soil evaporation, since it can only draw water from a quickly drying out top layer.

These results also show that basic simulation units are sufficient. The factors that really make a difference are rainfall, evapotranspiration, and the crop factors; stratifying the study into separate simulation units for other factors has little use. For example, the study area could also be divided into strata based on K_s, but the sensitivity analysis shows that the differences in recharge between those strata would be small. The uncertainty in recharge due to uncertain rainfall, evapotranspiration, and crop factors almost certainly dominates the small differences in recharge between strata based on other factors. Taking θ_S as the arithmic average is also somewhat justified: σ is relatively low, suggesting that the effect of θ_S on drainage is fairly linear.

The results of this sensitivity analysis generally agree with the sensitivity analyses of Jiménez-Martínez et al. (2009) and Lu et al. (2011), although K_s was not as unimportant as in this study.

One important assumption to interpret this sensitvity analysis is that SWAP is capable of simulating recharge well enough, so that factors which are most important in SWAP are also the most important in reality. This appears to be true, since SWAP (or a similar model like HYDRUS-1D) has been used for the purpose of estimating groundwater recharge, see Anuraga et al. (2006), Lu et al. (2011), Sarwar et al. (2000), Jiménez-Martínez et al. (2009), Ahmad et al. (2002). However, all these studies also have in common that soil hydraulic parameters were calibrated using measurements of soil pressure head and soil water content. This was outside of the scope of this studay. This raises an interesting issue: Lu et al. (2011) remark that 'initial simulations using the laboratory estimated unsaturated soil hydraulic parameters, or those estimated using pedotransfer functions, were found to be relatively poor and in need of improvement.' How important are these unsaturated soil hydraulic parameters for recharge? The results of the sensitivity analysis suggest that SWAP can be applied for estimating

groundwater recharge without measurement of soil moisture content and pressure heads for subsequent calibration of soil hydraulic parameters in areas comparable to St. Eustatius – as was done in this study – but it should be kept in mind that parameters have been perturbed only slightly, maximally 15%. Additionally, measuring field soil moisture contents and pressure heads allows to firmly ground the model in reality.

For the purpose of estimating groundwater recharge, I agree with the conclusions of Jiménez-Martínez et al. (2009): 'Future work aimed at quantifying uncertainty in parameter suchs as [the crop factor] or [reference evapotranspiration] would greatly benefit efforts to determine uncertainty in recharge calculations'. Further research is also especially needed for quantifying crop factors for natural vegetation. A list of crop factors for (classes of) natural vegetation, similar to the one for agricultural crops in Allen et al. (1998), would be extremely useful in groundwater recharge estimations. Additionally, more investigations to verify the accuracy of the FAO-56 method for estimating crop factors from vegetation height and vegetative soil cover or leaf area are needed.

I also conclude that prior to research careful consideration is required on how to prioritize which variables are measured. Whenever possible, a sensitivity analysis should be conducted to rank factors in order of importance, before a measurement plan is made. In many cases, if measurements are not (yet) available, variables can be estimated. Global datasets are available for (agro)meteorological conditions (e.g. Muñoz and Grieser (2006)), soil hydraulic properties can be determined using soil descriptions and pedotransfer functions, and vegetation parameters are generally taken from literature even in the final application. The measurement plan should be made on the basis of this a priori sensitivity analysis.

3.5.2 *Simulation of recharge*

Table 10 shows the groundwater recharge predicted by SWAP. The different vegetation characteristics only cause a small difference in recharge compared to differences in rain. However, when using the Gash interception model with the values found in Návar and Bryan (1994), Návar et al. (1999a) and Návar et al. (1999b) for the shrubland unit, recharge is decreased notably: the average yearly recharge for the three simulated rainfall scenarios is 59, 89, and 170 mm y^{-1} respectively. It is difficult to compare these values in table 10, because it is not clear how representative the values used in the Gash model are, but it demonstrates that rainfall interception requires more attention. The differences are relatively large compared to those in the sensitivity analysis, because the perturbations there did not involve switching interception models.

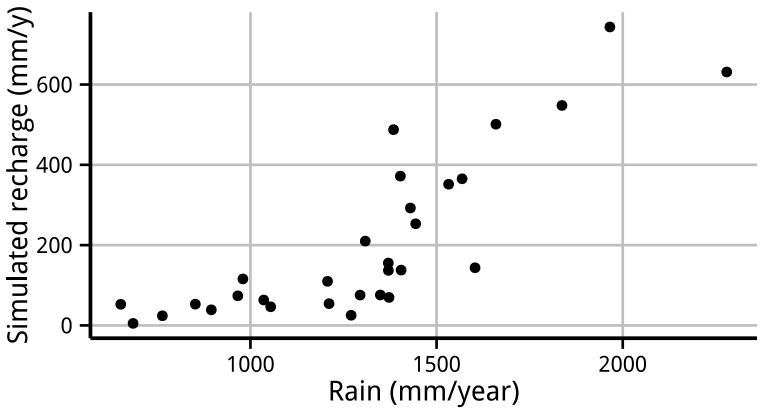

Figure 24: Yearly simulated recharge versus yearly rainfall of 30 years, for the shrubland simulation unit, average yearly rainfall of 1304 mm.

Figure 24 shows yearly simulated recharge versus yearly rainfall. In general, when yearly rainfall is roughly below 1300 mm little groundwater recharge is simulated, but the points do not fall on a single line: calculating groundwater recharge on St. Eustatius as a fraction of yearly rainfall will result in inaccurate estimates, emphasizing the importance of dynamic simulaton of recharge (Anuraga et al., 2006). Calculated average reference evapotranspiration amounts to 1970 mm per year, so rainwater will only pass through the unsaturated zone when rain intensities are large enough or when antecedent soil moisture is high enough.

Table 10: Average simulated groundwater recharge over the period 1 January 1984 to 31 December 2013 per simulation unit for three simulated rainfall scenarios. Between parentheses is recharge as a percentage of average annual rainfall.

	Average groundwater recharge (mm year^{-1})		
Simulation unit	980 mm year^{-1}	1089 mm year^{-1}	1304 mm year^{-1}
Airport	80 (8.1)	117 (10.7)	211 (16.2)
Pasture	80 (8.1)	117 (10.7)	211 (16.2)
Shrubland	77 (7.9)	113 (10.4)	207 (15.9)
Forest	75 (7.7)	109 (10.0)	200 (15.3)

Using the areas of table 2, volumes of groundwater recharge can be calculated, see table 11[1]. While the roofs constitute 2.1% of the

1 This is the quantity of groundwater recharge for the *entire* study area. It is not clear whether this all of this water ends up recharging the (part of) the aquifer that is used and influenced by the people of St. Eustatius, because groundwater flow patterns are unknown. See the discussion under the section Groundwater.

study area, sewage water might generate as much as a fifth of the groundwater recharge in the study area. This portion is almost certainly overestimated, since water is lost from the moment the rain falls on the roofs to the moment it infiltrates in a cesspit and these losses have not been determined; additional research is required to determine sewage water quantities. However, infiltrating sewage water does likely contribute an important portion to groundwater recharge: research in the Bahamas showed also that infiltrating sewage water and storm soakaways increased recharge by over 200 mm y^{-1} in urban areas, from 365 mm y^{-1} to 575 mm y^{-1} (Thomson and Foster (1986) in Lerner (1990)).

Table 11: Volume of average yearly groundwater recharge over the period 1 January 1984 to 31 December 2013 for three simulated rainfall scenarios.

	Average groundater recharge (10^4 m^3 $year^{-1}$)		
Origin	980 mm $year^{-1}$	1089 mm $year^{-1}$	1304 mm $year^{-1}$
Natural	68	99	181
Cesspit	19	21	25
Total	87	120	206

The output of the SWAP model shows that precipitation intensity and especially antecedent soil moisture play a crucial role in generating drainage. Figure 25 shows an example. A major precipitation peak of 183 mm can be identified at April 1997, but drainage shows only a small signal as the water is simply stored in the soil. The earlier precipitation events in the second half of 1995 do result in drainage peaks of over 10 mm d^{-1}, as soil water storage is high enough. At a glance, a threshold can be drawn at roughly 200 mm of storage. When storage exceeds roughly 200 mm, drainage is generated.

In fact, the drainage output of the SWAP model can be simulated quite well with a linear reservoir model. The behaviour can described as follows: rain fills up a reservoir (the soil), and evapotranspiration continually empties this reservoir. Only when a critical storage level in the reservoir is exceeded is drainage really generated. Ignoring runoff, as has also been done in the SWAP simulations, the water balance takes the form

$$P - ET_a - D = \Delta S \tag{17}$$

where P (mm d^{-1}) is rainfall, ET_a is evapotranspiration (mm d^{-1}), D (mm d^{-1}) is drainage, and ΔS (mm d^{-1}) is storage change. ET is calculated as

$$ET_a = \min(k_{ET}\, S, ET_p) \tag{18}$$

where k_{ET} (d^{-1}) is an empirical constant, describing the dependency of ET on storage S, and ET_p (mm) is potential evapotranspiration. For

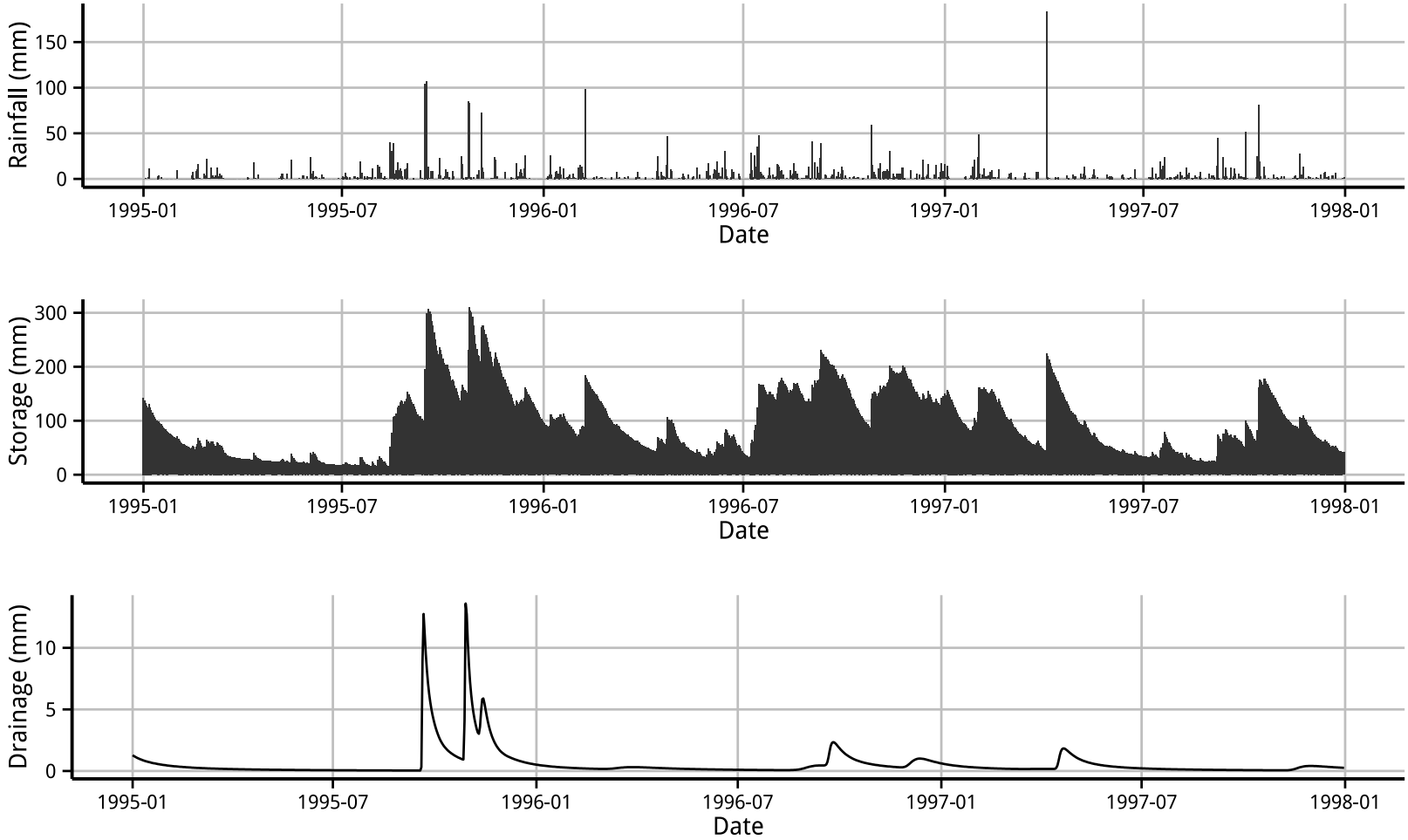

Figure 25: Precipitation, and storage and drainage simulated by SWAP for the shrubland simulation unit for the period 1 January 1995 to 1 January 1998.

Table 12: Reservoir model parameter ranges, increments, and optimal values. Optimal value is based on mean absolute error.

Parameter	Range	Increment	Optimal value
k_{ET}	0.020–0.080	0.005	0.040
ET_p	3.00–5.00	0.25	4.75
S_{crit}	150–250	25	175

simplicity ET_p is assumed constant here, which is somewhat justified given the tropical climate. ET increases with S, up to the level where it comes potential, ET_p. Drainage is calculated as

$$D = \max(S - S_{crit}, 0) \tag{19}$$

where S_{crit} (mm) is the critical soil water storage upon which drainage begins.

The model uses an explicit method with a daily resolution to calculate ET and D: for timestep t, $ET(t)$ and $D(t)$ are calculated using $S(t-1)$.

Drainage can be estimated in a simple manner with this model, which requires only daily precipitation data. Three parameters, k_{ET}, ET_p, and S_{crit} are enough to get a basic functionality that results in yearly drainage that greatly resembles the SWAP results. The optimal values of these parameters have been determined in terms of mean absolute error in yearly recharge using a combinatorial approach, by generating an array of possible values for each parameters, and testing all combinations. See table 12.

The results can be seen in figure 26. The reservoir model underestimates groundwater recharge for a few of the driest years, as shown by by the collection of points in the bottom left corner. The difference is that a slight amount of drainage is generated by SWAP even in dry years: there is always some water that trickles down. The reservoir model, on the other hand, is binary in the sense that if S_{crit} is not exceeded no drainage is generated. For the scenarios of 980 and 1089 mm average annual rainfall, R^2 is respectively 0.94 and 0.95; R^2 increases with average annual rainfall since the steady trickle becomes less important in proportion to rainfall events.

When storage exceeds the threshold, the excess storage is immediately removed to produce drainage. An attenuated drainage pattern can be produced by including a second reservoir from which the water would slowly drain. A second linear reservoir has been included to produce figure 27, so simulated drainages can be compared (the second linear reservoir has a coefficient of 0.4: $D = 0.4S_2$, where S_2 is the storage level of the second reservoir). The reservoir model does an adequate job in reproducing drainage pattern generated by SWAP. The difference is the response time of the reservoir model (peakiness),

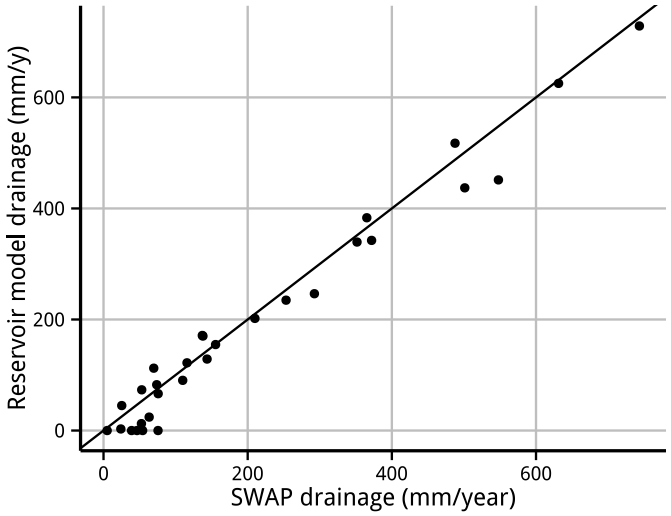

Figure 26: Yearly recharge simulated by SWAP versus yearly recharge simulated by the reservoir model, for the shrubland simulation unit, average yearly rainfall of 1304 mm. R^2 = 0.97, MAE = 27 mm y^{-1}.

which is unavoidable without finer temporal discretization. From the yearly perspective, a second reservoir is unnecessary: drainage quantities are not different (unless a route back to the first reservoir is included).

Of course, some reservations are appropriate. The SWAP model is already simplified by assuming constant vegetation characteristics and by ignoring hysteris and macropore flow. While the hydrological functioning of the top three meters of the soil appears to be captured quite well by this conceptual model, actual soil moisture measurements would be required for real validation.

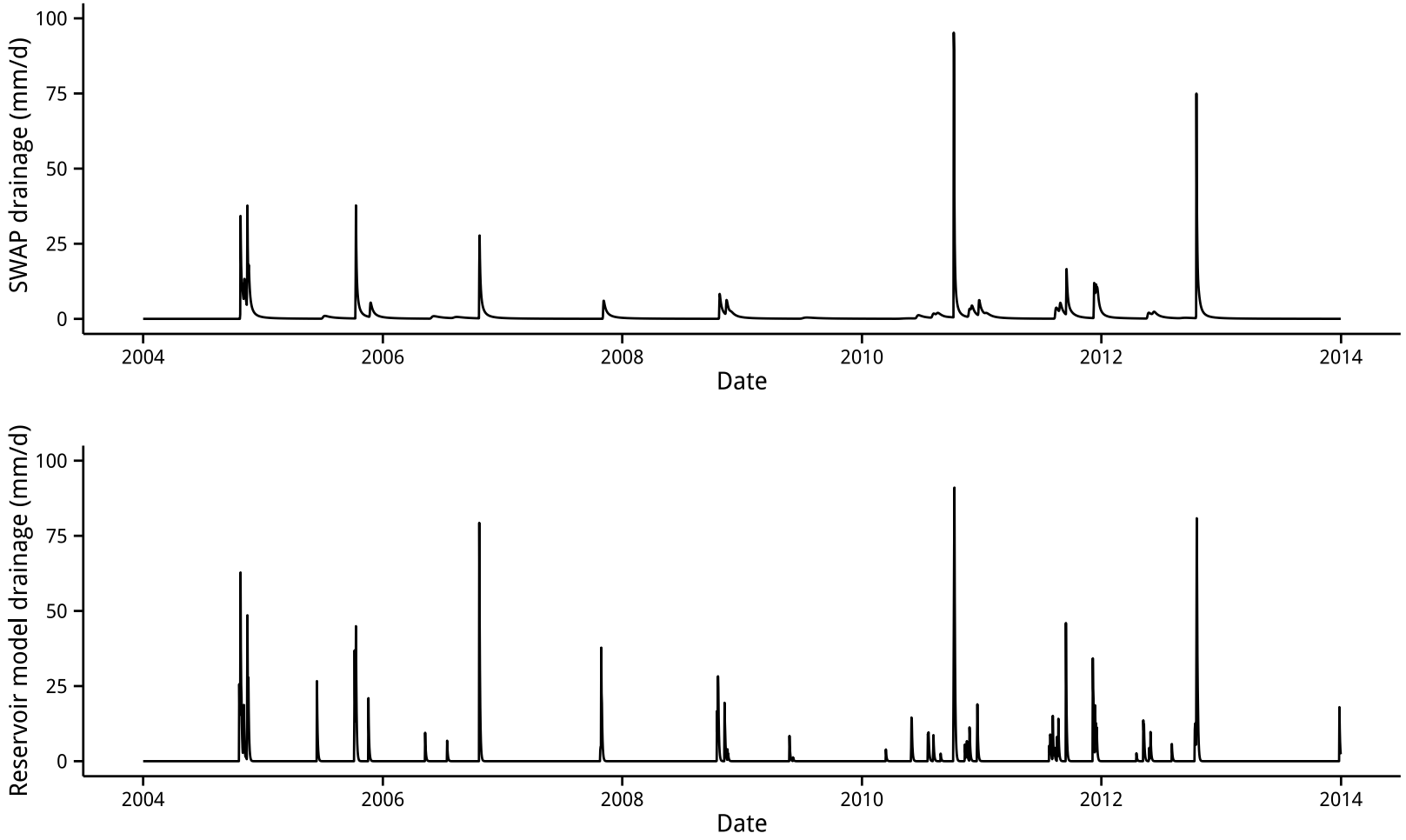

Figure 27: Daily drainage as simulated by SWAP and the reservoir model for the period 1 January 2004 to 1 January 2014.

3.6 GROUNDWATER

Groundwater levels

Calculating recharge based on groundwater levels is not feasible for this study. Of the four Divers three of these cannot be used either because they are regularly used for groundwater extraction (wells 9, 13) or because of proximity to the sea (well 3, 13). The fourth well (8) is not (regularly) used for groundwater extraction and features groundwater at a depth of circa 55 meters below ground level (which is representative for most of the aquifer in the study area).

Groundwater levels observed in well 8 for the period May 2014 to January 2015 show no sudden response to a rainfall event. This means that a groundwater fluctuation method (Healy, 2010) is not suitable for the avaliable data. The lack of rainfall response is either because the recharge is diffuse, the recharge is attenuated, or because there simply has not been a rainfall event large enough to pass through the first meters of the soil; the reservoir model confirms that a storage of circa 175 mm needs to be exceeded before drainage occurs. To exceed such a storage, large rainfall events are required, such as storms. These likely cover the entire island so that recharge arriving at the water table is likely focused, not diffuse – unlike the influence of infiltrating sewage. Furthermore, lag times between precipitation and groundwater level response can be large, up to many years (Rossman et al., 2014), depending on conductivity and depth to the groundwater table. The lag for deep groundwater at St. Eustatius is likely sizeable, given the depth to the groundwater table. The size of this lag cannot be determined due to the short measuring period for groundwater levels. The groundwater level could also be affected by drawdown of nearby wells: the nearest well used for extraction is 750 m away and is regularly used.

Therefore, if groundwater levels are recorded, this should also occur for long periods. With a large lag time in the groundwater response to precipitation, the groundwater response to a precipitation event cannot be identified for short timeseries. In practical terms, these measurements should be made in wells that are not used for groundwater extraction, and that are closed so it cannot rain into the well. One interesting phenomenon not investigated in this thesis is the attenuation of tidal fluctuations in the wells; simulation of groundwater waves using the approach of e.g. Nielsen et al. (1997) might be used to estimate the hydraulic conductivity of the aquifer.

One approach to estimate groundwater response lag is to simply model the entire unsaturated zone. However, it seems unlikely that simulating the entire 55 meters of the unsaturated zone would result in an accurate prediction of the groundwater response lag due to the unknown properties of the subsoil. For example, Verhagen et al.

(2014) attempted to estimate the response time of the groundwater table under an unsaturated zone of 70 m in the Veluwe using the model HYDRUS 1D (Simunek et al., 2008): the model predicted a delay of 61 months while the observed delay was only 8 to 10 months. Preferential flow likely plays an important role, but it cannot reliably be predicted without deep knowledge of the subsoil.

One important question is what the shape of the water table is and which areas are recharging the Cultuurvlakte groundwater. The shape of the groundwater table is not necessarily a subdued replica of the topgraphy (Haitjema and Mitchell-Bruker, 2005). The shape might depend strongly on the location and the conductivity of the andesitic dome that is underneath the Quill. If the dome extends to the north to the center of the crater, and is impermeable, the Quill will likely recharge the Cultuurvlakte. If the dome is found only under the White Wall formation, or if it is highly permeable, the groundwater might directly flow into the sea without passing through a part of the Cultuurvlakte. In that case, assuming uniform hydraulic conductivity, the groundwater likely flows in a radial pattern with the highest water table somewhere under the Cultuurvlakte.

Similarly, the northern hills may also play a role in recharging the Cultuurvlakte. The soil on the hills is clayey (Augustinus et al., 1985) with relatively low hydraulic conductivity and the hills are steep, so that some runoff may be generated which flows downhill and infiltrates at the foot of the hill. A more important unknown is the behaviour of the groundwater in andesite domes. Fractures in rock determine groundwater flow direction and magnitude, but estimating fractured bedrock hydraulic conductivity is not straightfoward (Voeckler and Allen, 2012) and was outside of the scope of this research. There are some recognizable streams in the northern hills, so I speculate that infiltrability may be small(er) that and therefore little groundwater recharge occurs in the northern hills: during my stay I have only witnessed natural surface water in the northern hills and nowhere else on the island. The results of the chemical analysis also seem to support the notion that flow is not towards the hills, see below.

Measuring groundwater levels would be the most straightforward way of estimating the shape of the water table and the direction of groundwater flow. The measured depths so far are not measured to a single accurate reference, and therefore effectively unusable to estimate the shape of the water table.

Chemical analysis

The unknowns with regards to groundwater flow make it currently impossible to determine a source area for the groundwater. However, by assuming the source area is local, a recharge estimate can be made

by using nitrogen as a tracer: in groundwater samples taken from some wells on St. Eustatius, very high nitrogen concentrations can be found. This nitrogen originates from domestic wastewaster infiltrating in cesspits in residential areas. See table 13 for nitrogen content in the sampled groundwater. Wells in residential areas (9, 1, 6, 8, 2) show the highest nitrogen contents. Low nitrogen concentrations in wells 5, 10, and 11 suggest that groundwater flow is not northward from the residential areas towards the northern hills.

The amount of nitrogen can quantified by estimating the quantity of water infiltrating – assumed to be equal to the rainfall falling on roofs – and the nitrogen content of this water. Let us assume sewage water has a total nitrogen concentration of 60 mg L^{-1} (Reay, 2004). The groundwater at well 1 has a total nitrogen concentration of about 30 mg L^{-1}. Assuming natural groundwater recharge has a concentration of 0 mg L^{-1} and the groundwater is well mixed, the groundwater at this well exists of half wastewaster, half natural recharge. If we assume that the water divide is roughly in the center of the Cultuurvlakte, then the source area of this well roughly corresponds with the Oranjestad landscape unit (unit 16 in figure 8). With 10% of the Oranjestad area covered by roof recharging on average 1300 mm $year^{-1}$, a natural recharge of 144 mm is required for this mixing ratio, which is within the ranges of the SWAP predictions.

Table 13: Total inorganic nitrogen for sampled wells.

Well	N (mg L^{-1})
9	49.70
1	34.13
6	27.64
8	20.38
2	16.63
7	15.19
13	9.64
3	4.81
4	2.98
12	1.65
10	1.51
5	0.01
11	0.05

While these results confirm the simulated recharge, this calculation is obviously very rough. Reay (2004) mention that sewage water nitrogen content varies between 35 to 100 mg L^{-1}. Of the other two wells in the area (2 and 6), the nitrogen contents of the groundwater are 17 and 28 mg L^{-1} respectively, so the nitrogen content of the groundwater is uncertain too. The number for the quantity of sewage water is almost certainly too high: not all the rain in a year will end up as sewage water. The largest uncertainty lies in the spatial extent of the source area. Regardless, the calculated estimate agrees in terms of order of magnitude. These data suggest that in some areas a large portion (a third to all) of the groundwater recharge is indeed infiltrated sewage water.

4

CONCLUSIONS AND RECOMMENDATIONS

Based on the results of the 30 year simulation, long term natural average groundwater recharge ranges from 75 to 210 mm y^{-1}, or 8% to 16% of average yearly rainfall. A back-of-the-envelope calculation using observed nitrogen levels in groundwater also results in a recharge between those bounds. Average annual volumes of groundwater recharge for the study area ranges from 900 000 to 2 100 000 m^3 y^{-1}. Nearly all of this water will end up discharging into the sea, but flow paths are unknown. More research into the hydrogeology is required to estimate routes the water follows after it reaches the water table. Accurate longterm groundwater depth measurements (relative to a single reference) in all wells may be a valuable first step.

Rainfall is the most important factor in determining groundwater recharge, followed by reference evapotranspiration and vegetation characteristics that control evapotranspirative fluxes. The importance of other factors was relatively minor in comparison. A conceptual reservoir model with one input variable, rainfall, and four parameters can mimick SWAP drainage output quite succesfully for St. Eustatius. Rain fills this reservoir, which is continually emptied by evapotranspiration. When a critical storage level is exceeded, the reservoir 'overflows' and drainage is generated, so that rain intensity and antecedent soil moisture play a crucial role in determining drainage. Infiltrating sewage water in cesspits is likely a sizeable part of groundwater recharge. It has a relatively direct route into the groundwater since it is not subject to interception or transpiration by vegetation. Accurate determination of the quantity of sewage water should be a topic of further research.

For St. Eustatius more rainfall measurements are required, especially on the lower parts of the Cultuurvlakte. Multiple rain gauges recording rainfall over a long period – decades – would allow to draw conclusions with regards to the size of the orographic effect and better guarantee the representativity of assumed rainfall in water budget calculations. More research into the vegetation that also investigates seasonal variation would also be beneficial – the potential for improvement is limited, however, without addtional research into the transpiration of natural vegetation.

In terms of alternative ways of estimating groundwater recharge, tracer methods come to mind, but given the irregular nature of precipitation this may prove challenging: years might go by, with little movement followed by a sudden washout. Chloride mass balance methods are almost certainly infeasible due to the intrusion of salt from seawa-

ter. Based on the period that groundwater levels were measured for this study, I cannot make conclusive statements about whether water table based methods are feasible or not: precipitation pulses may be so attenuated that they cannot be recognized in the movement of the water table, or groundwater recharge is diffuse, or no significant drainage was generated during the measurement period. Long term groundwater observations would therefore at least prove helpful to gain some understanding of the hydrological functioning of the island.

For improvement of a numerical simulation of the unsaturated zone, lab analysis of soil samples to determine soil hydraulic properties would be useful. Monitoring of pressure heads and soil water contents in the field would allow for some callibration of soil properties and to keep the SWAP grounded in reality. More thorough investigations of rooting distributions and interception parameters are also obvious improvements, but given the results of the sensitivity analysis, long term rainfall data collection should absolutely be prioritized.

Groundwater recharge estimation in general would be greatly facilitated by a dataset that allows to estimate evapotranspiration for natural vegetation. The FAO-56 method for estimating crop factors based on vegetation height and soil cover is very useful, but strongly needs to be validated in more research. Further research into vegetation transpiration is also especially important to give quantitative uncertainty bounds on groundwater recharge estimations.

Finally, I recommend that for groundwater recharge modeling studies, inputs are estimated a priori based on literature or databases, and that a sensitivity analysis is performed before fieldwork is planned. Inputs should be ranked according to importance based on the outcomes of the sensitivity analysis, so that attention can be distributed accordingly.

REFERENCES

Ahmad, M.-u.-D., Bastiaanssen, W., and Feddes, R. (2002). Sustainable use of groundwater for irrigation: a numerical analysis of the subsoil water fluxes. *Irrigation and Drainage*, 51(3):227–241.

Allen, R., Pruitt, W., Businger, J., Fritschen, L., Jensen, M., and Quinn, F. (1996). Chapter 4 'Evaporation and transpiration' in ASCE Handbook of Hydrology. *New York, NY*, pages 125–252.

Allen, R. G., Pereira, L., Raes, D., and Smith, M. (1998). FAO Irrigation and drainage paper No. 56. *Rome: Food and Agriculture Organization of the United Nations*, pages 26–40.

Allen, R. G. and Pereira, L. S. (2009). Estimating crop coefficients from fraction of ground cover and height. *Irrigation Science*, 28(1):17–34.

Anuraga, T., Ruiz, L., Kumar, M. M., Sekhar, M., and Leijnse, A. (2006). Estimating groundwater recharge using land use and soil data: A case study in South India. *agricultural water management*, 84(1):65–76.

Augustinus, P., Mees, R., and Prins, M. (1985). Biotic and abiotic components of the landscapes of St. Eustatius. *Eustatius (Netherlands Antilles). Uitgaven Nat. Wet. Studiekr. Sur. & NA*.

Bing Maps (2014). St. Eustatius. [Online; accessed September-2014 at `http://www.bing.com/maps/#Y3A9NTEuOTc1ODAwfjUuNjU0NzAwJmx2bD03JnN0eT1yJndoZXJlMT1TdC4lMjBFdXN0YXRpdXM=`].

Booth, D. T., Cox, S. E., and Berryman, R. D. (2006). Point sampling digital imagery with 'SamplePoint'. *Environmental Monitoring and Assessment*, 123(1-3):97–108.

Braak, C. (1935). *Het klimaat van Nederlandsch West-Indie*. Rijksuitgeverij.

Bristow, K. L. and Campbell, G. S. (1984). On the relationship between incoming solar radiation and daily maximum and minimum temperature. *Agricultural and forest meteorology*, 31(2):159–166.

Campolongo, F., Cariboni, J., and Saltelli, A. (2007). An effective screening design for sensitivity analysis of large models. *Environmental modelling & software*, 22(10):1509–1518.

Carrera-Hernández, J., Smerdon, B., and Mendoza, C. (2012). Estimating groundwater recharge through unsaturated flow modelling:

Sensitivity to boundary conditions and vertical discretization. *Journal of Hydrology*, 452:90–101.

Centraal Bureau voor de Statistiek (2014). Caribisch Nederland; bevolking (1 januari); geslacht, leeftijd. [Online; accessed 11-September-2014 at `http://statline.cbs.nl/StatWeb/publication/?DM=SLNL&PA=80534NED&D1=a&D2=0&D3=a&D4=2&D5=8-12&VW=T`].

Charlier, J.-B., Lachassagne, P., Ladouche, B., Cattan, P., Moussa, R., and Voltz, M. (2011). Structure and hydrogeological functioning of an insular tropical humid andesitic volcanic watershed: A multi-disciplinary experimental approach. *Journal of Hydrology*, 398(3):155–170.

De Freitas, J., Rojer, A., Nijhof, B., and Debrot, A. (2012). A landscape ecological vegetation map of Sint Eustatius (Lesser Antilles). *Wageningen: IMARES Wageningen UR*.

Decagon Devices (2011). Mini Disk Infiltrometer User's Manual Version 9.

Descheemaeker, K., Raes, D., Allen, R., Nyssen, J., Poesen, J., Muys, B., Haile, M., and Deckers, J. (2011). Two rapid appraisals of FAO-56 crop coefficients for semiarid natural vegetation of the northern Ethiopian highlands. *Journal of Arid Environments*, 75(4):353–359.

Dillon, P. (1997). *Groundwater pollution by sanitation on tropical islands*. Unesco Paris.

Donatelli, M. and Bellocchi, G. (2001). Estimate of daily global solar radiation: new developments in the software RadEst3.00. In *Proceedings of the 2nd International Symposium on Modelling Cropping Systems, Florence, Italy*, pages 16–18.

Donatelli, M. and Campbell, G. (1998). A simple model to estimate global solar radiation. In *Proceedings of the Fifth European Society of Agronomy Congress*, volume 2, pages 133–134.

Droogers, P. and Allen, R. G. (2002). Estimating reference evapotranspiration under inaccurate data conditions. *Irrigation and drainage systems*, 16(1):33–45.

ESRI (2011). ArcGIS Desktop: Release 10.

Fayer, M. and Hillel, D. (1986). Air encapsulation: I. Measurement in a field soil. *Soil Science Society of America Journal*, 50(3):568–572.

Fetter, C. (1972). Position of the saline water interface beneath oceanic islands. *Water Resources Research*, 8(5):1307–1315.

Gleick, P. H. et al. (1993). *Water in crisis: a guide to the world's fresh water resources.* Oxford University Press, Inc.

Haitjema, H. M. and Mitchell-Bruker, S. (2005). Are water tables a subdued replica of the topography? *Groundwater*, 43(6):781–786.

Hargreaves, G. H. and Allen, R. G. (2003). History and evaluation of Hargreaves evapotranspiration equation. *Journal of Irrigation and Drainage Engineering*, 129(1):53–63.

Harmsen, E. W. (2003). Fifty years of crop evapotranspiration studies in Puerto Rico. *Journal of soil and water conservation*, 58(4):214–223.

Healy, R. W. (2010). *Estimating groundwater recharge*. Cambridge University Press.

Hlaváčiková, H. and Novák, V. (2014). A relatively simple scaling method for describing the unsaturated hydraulic functions of stony soils. *Journal of Plant Nutrition and Soil Science*, 177(4):560–565.

Hodnett, M. and Tomasella, J. (2002). Marked differences between van Genuchten soil water-retention parameters for temperate and tropical soils: a new water-retention pedo-transfer functions developed for tropical soils. *Geoderma*, 108(3):155–180.

Hopmans, J. W., Nielsen, D. R., and Bristow, K. L. (2002). How useful are small-scale soil hydraulic property measurements for large-scale vadose zone modeling? *Environmental Mechanics: Water, Mass and Energy Transfer in the Biosphere: The Philip Volume*, pages 247–258.

Howarth, R. W. and Marino, R. (2006). Nitrogen as the limiting nutrient for eutrophication in coastal marine ecosystems: evolving views over three decades. *Limnology and Oceanography*, 51(1):364–376.

Jiménez-Martínez, J., Skaggs, T., Van Genuchten, M. T., and Candela, L. (2009). A root zone modelling approach to estimating groundwater recharge from irrigated areas. *Journal of Hydrology*, 367(1):138–149.

Kelliher, F., Leuning, R., and Schulze, E. (1993). Evaporation and canopy characteristics of coniferous forests and grasslands. *Oecologia*, 95(2):153–163.

Kroes, J., Van Dam, J., Groenendijk, P., Hendriks, R., and Jacobs, C. (2009). *SWAP version 3.2: Theory description and user manual*. Alterra Wageningen, The Netherlands.

Lachassagne, P., Aunay, B., Frissant, N., Guilbert, M., and Malard, A. (2014). High-resolution conceptual hydrogeological model of complex basaltic volcanic islands: a Mayotte, Comoros, case study. *Terra Nova*.

Langensiepen, M., Fuchs, M., Bergamaschi, H., Moreshet, S., Cohen, Y., Wolff, P., Jutzi, S. C., Cohen, S., Rosa, L. M. G., Li, Y., et al. (2009). Quantifying the uncertainties of transpiration calculations with the Penman-Monteith equation under different climate and optimum water supply conditions. *Agricultural and forest meteorology*, 149(6):1063–1072.

Lerner, D. N. (1990). Groundwater recharge in urban areas. *Atmospheric Environment. Part B. Urban Atmosphere*, 24(1):29–33.

Lhomme, J. P., Montes, C., Jacob, F., and Prévot, L. (2013). Evaporation from multi-component canopies: Generalized formulations. *Journal of Hydrology*, 486:315–320.

Lu, X., Jin, M., van Genuchten, M. T., and Wang, B. (2011). Groundwater recharge at five representative sites in the Hebei Plain, China. *Groundwater*, 49(2):286–294.

Martinelli, L. A., Howarth, R. W., Cuevas, E., Filoso, S., Austin, A. T., Donoso, L., Huszar, V., Keeney, D., Lara, L. L., Llerena, C., et al. (2006). Sources of reactive nitrogen affecting ecosystems in Latin America and the Caribbean: current trends and future perspectives. In *Nitrogen Cycling in the Americas: Natural and Anthropogenic Influences and Controls*, pages 3–24. Springer.

Morris, M. D. (1991). Factorial sampling plans for preliminary computational experiments. *Technometrics*, 33(2):161–174.

Mualem, Y. (1976). A new model for predicting the hydraulic conductivity of unsaturated porous media. *Water resources research*, 12(3):513–522.

Muñoz, G. and Grieser, J. (2006). Climwat 2.0 for CROPWAT. *Food and Agriculture Organization, Rom*.

National Oceanic and Atmospheric Administration (2014). Daily Observational Data. [Online; accessed 18-November-2014 at `http://gis.ncdc.noaa.gov/map/viewer/#app=clim&cfg=cdo&theme=daily&layers=0001&node=gis`].

Návar, J. and Bryan, R. B. (1994). Fitting the analytical model of rainfall interception of Gash to individual shrubs of semi-arid vegetation in northeastern Mexico. *Agricultural and Forest Meteorology*, 68(3):133–143.

Návar, J., Carlyle-Moses, D. E., and Martinez, A. (1999a). Interception loss from the Tamaulipan matorral thornscrub of north-eastern Mexico: an application of the Gash analytical interception loss model. *Journal of Arid Environments*, 41(1):1–10.

Návar, J., Charles, F., and Jurado, E. (1999b). Spatial variations of interception loss components by Tamaulipan thornscrub in northeastern Mexico. *Forest Ecology and Management*, 124(2):231–239.

Nielsen, P., Aseervatham, R., Fenton, J. D., and Perrochet, P. (1997). Groundwater waves in aquifers of intermediate depths. *Advances in Water Resources*, 20(1):37–43.

Palm, J. d. (1985). *Encyclopedie van de Nederlandse Antillen*. Zutphen: Walburg Pers.

Philip, J. (1980). Field heterogeneity: some basic issues. *Water Resources Research*, 16(2):443–448.

Pinto-Coelho, R., Bezerra-Neto, J., et al. (2005). Effects of eutrophication on size and biomass of crustacean zooplankton in a tropical reservoir. *Brazilian Journal of Biology*, 65(2):325–338.

R Core Team (2014). *R: A Language and Environment for Statistical Computing*. Vienna, Austria.

Rad, S. D., Allègre, C. J., and Louvat, P. (2007). Hidden erosion on volcanic islands. *Earth and Planetary Science Letters*, 262(1):109–124.

Reay, W. G. (2004). Septic tank impacts on ground water quality and nearshore sediment nutrient flux. *Groundwater*, 42(7):1079–1089.

Ringersma, J. and Sikking, A. (2001). Determining transpiration coefficients of Sahelian vegetation barriers. *Agroforestry systems*, 51(1):1–9.

Rojer, A. (1997). Biological inventory of Sint Eustatius. *Unpubl. Report, Carmabi Foundation, KNAP Project*, pages 96–10.

Roobol, M. J. and Smith, A. L. (2004). *Volcanology of Saba and St. Eustatius, Northern Lesser Antilles*.

Rossman, N., Zlotnik, V. A., Rowe, C., and Szilagyi, J. (2014). Vadose zone lag time and potential 21st century climate change effects on spatially distributed groundwater recharge in the semi-arid Nebraska Sand Hills. *Journal of Hydrology*, 519:656–669.

Ruano, M., Ribes, J., Seco, A., and Ferrer, J. (2012). An improved sampling strategy based on trajectory design for application of the morris method to systems with many input factors. *Environmental Modelling & Software*, 37:103–109.

Saltelli, A., Tarantola, S., Campolongo, F., and Ratto, M. (2004). *Sensitivity analysis in practice: a guide to assessing scientific models*. John Wiley & Sons.

Sarwar, A., Bastiaanssen, W., Boers, T. M., and Van Dam, J. (2000). Evaluating drainage design parameters for the fourth drainage project, Pakistan by using SWAP model: Part I–Calibration. *Irrigation and Drainage Systems*, 14(4):257–280.

Scanlon, B. R., Reedy, R. C., Stonestrom, D. A., Prudic, D. E., and Dennehy, K. F. (2005). Impact of land use and land cover change on groundwater recharge and quality in the southwestern us. *Global Change Biology*, 11(10):1577–1593.

Schaap, M. G., Leij, F. J., and van Genuchten, M. T. (2001). ROSETTA: a computer program for estimating soil hydraulic parameters with hierarchical pedotransfer functions. *Journal of hydrology*, 251(3):163–176.

Schenk, H. J. and Jackson, R. B. (2002). The global biogeography of roots. *Ecological monographs*, 72(3):311–328.

Simunek, J., Sejna, M., Saito, H., Sakai, M., and van Genuchten, M. T. (2008). The HYDRUS-1D software package for simulating the movement of water, heat, and multiple solutes in variably saturated media, version 4.0, HYDRUS software series 3. *Department of Environmental Sciences, University of California Riverside, Riverside, California, USA*, page 315.

Smith, R. B., Schafer, P., Kirshbaum, D., and Regina, E. (2009a). Orographic enhancement of precipitation inside Hurricane Dean. *Journal of Hydrometeorology*, 10(3):820–831.

Smith, R. B., Schafer, P., Kirshbaum, D. J., and Regina, E. (2009b). Orographic precipitation in the tropics: Experiments in Dominica. *Journal of the atmospheric sciences*, 66(6):1698–1716.

Smith, S., Muecher, C., Debrot, A. O., Roupioz, L., Meesters, H. W. G., Hazeu, G., and Davaasuren, N. (2013). Use of satellite data for the monitoring of species on Saba and St. Eustatius. Technical report, IMARES.

Sobel, A. H., Burleyson, C., and Yuter, S. (2011). Rain on small tropical islands. *Journal of Geophysical Research: Atmospheres (1984–2012)*, 116(D8).

Suehrcke, H. (2000). On the relationship between duration of sunshine and solar radiation on the earth's surface: Angström's equation revisited. *Solar Energy*, 68(5):417–425.

Tabari, H., Grismer, M. E., and Trajkovic, S. (2013). Comparative analysis of 31 reference evapotranspiration methods under humid conditions. *Irrigation Science*, 31(2):107–117.

Ten Harkel, W. (2015). Runoff and erosion on the Cultuurvlakte of St. Eustatius. Master's thesis.

Thomson, J. and Foster, S. (1986). Effect of urbanization on groundwater of limestone islands: an analysis of the Bermuda case. *Journal of the Institution of Water Engineers and Scientists*, 40(6):527–540.

Thornton, P. E. and Running, S. W. (1999). An improved algorithm for estimating incident daily solar radiation from measurements of temperature, humidity, and precipitation. *Agricultural and Forest Meteorology*, 93(4):211–228.

Van der Velde, J., Hoogenboezem-Lanslots, K., Schenau, Y., Van Leeuwen, R., Briene, M., and De Freitas, J. (2010). St. Eustatius Development Plan.

Vandervaere, J.-P., Vauclin, M., and Elrick, D. E. (2000). Transient flow from tension infiltrometers I. The two-parameter equation. *Soil Science Society of America Journal*, 64(4):1263–1272.

Veenenbos, J. (1955). A soil and land capability survey of St. Maarten, St. Eustatius and Saba, Netherlands Antilles. *Publications for the foundation for scientific research in Surinam and the Netherlands Antilles*, 11.

Verhagen, F., Spek, T., Witte, F., Voortman, B., Moors, E., and Querner, E. (2014). Begrijpen we het watersysteem? *Stromingen*, 20(03):49–63.

Voeckler, H. and Allen, D. (2012). Estimating regional-scale fractured bedrock hydraulic conductivity using discrete fracture network (DFN) modeling. *Hydrogeology Journal*, 20(6):1081–1100.

Wageningen UR (2013). Zero nutrient discharge and total reuse of nutrients. [Online; accessed 24-September-2014 at `http://www.wageningenur.nl/nl/show/Zero-nutrient-discharge-and-total-reuse-of-nutrients.htm`].

Westermann, J. H. and Kiel, H. (1961). *The Geology of Saba and St. Eustatius: With Notes on the Geology of St. Kitts, Nevis and Montserrat (Lesser Antilles)*. Natuurwetenschappelijke Studiekring voor Suriname en de Nederlandse Antillen.

Zhang, R. (1997). Determination of soil sorptivity and hydraulic conductivity from the disk infiltrometer. *Soil Science Society of America Journal*, 61(4):1024–1030.

A

APPENDIX A: SWAP AND FAO-56 CROP FACTORS

This appendix deals with how a crop coefficient calculated with FAO-56 methods can be used in SWAP. In the SWAP Theory description and user manual (Kroes et al., 2009), the ratio of potential crop evapotranspiration over reference evapotranspiration (ET_p/ET_{ref}) is called the crop *factor* K_c. In FAO-56 this is called the crop *coefficient*. These terms may be used interchangeably, but for clarity I will use the term factor when referring to SWAP, and the term coefficient for FAO-56; idem ditto for FAO-56 effective fraction of ground cover $f_{c,eff}$ and SWAP soil cover SC.

Crop factors and crop coefficients

In SWAP three evapotranspiration concepts are explicitly specified:

- ET_{ref}: evapotranspiration rate of a reference crop (generally grass), kept at a constant height and well watered.
- ET_p: evapotranspiration rate of a selected crop, without water stress. Calculated as $ET_p = K_c ET_{ref}$.
- ET_a: actual evapotranspiration rate of the selected crop, possibly reduced by water stress.

FAO-56 presents two approaches for calculating crop evapotranspiration ET_p from a reference evapotranspiration ET_{ref}: with a single crop coefficient or with a dual crop coefficient.

In the single crop coefficient approach, potential crop evapotranspiration is calculated with

$$ET_p = K_c ET_{ref} \tag{20}$$

where ET_c (mm d^{-1}) is the potential crop evapotranspiration, K_c (-) is the crop coefficient, and ET_{ref} (mm d^{-1}) is the reference evapotranspiration. Here, both crop transpiration and soil evaporation are integrated into a single coefficient, averaging the effect of wetting.

In the dual crop coefficient approach, the crop coefficient is split in two: one for the basal crop (K_{cb}) and one for soil evaporation (K_e). Potential crop evapotranspiration is calculated with

$$ET_c = (K_{cb} + K_e) ET_{ref} \tag{21}$$

where K_{cb} (-) is the basal crop coefficient and K_e (-) the soil evaporation coefficient. K_{cb} is the ratio of the crop evapotranspiration over the reference evapotranspiration (ET_c/ET_{ref}) when the soil surface is

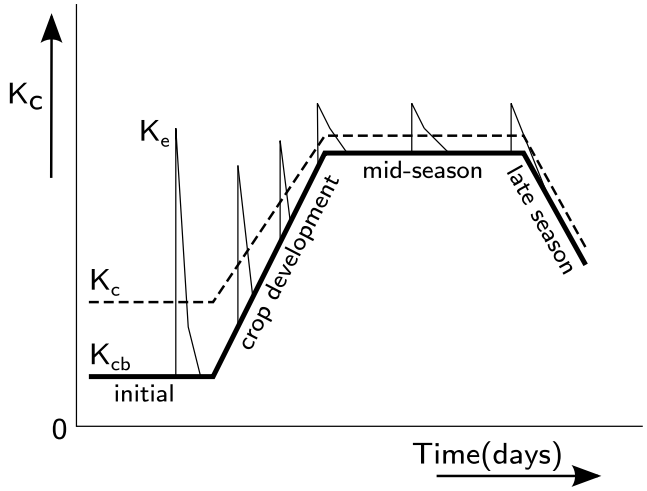

Figure 28: Example crop coefficient curves showing basal K_{cb} (thick line), soil evaporation K_e (thin line) and the corresponding single crop coefficient $K_c = K_{cb} + \overline{K_e}$. Adapted from Allen et al. (1998).

dry, but when transpiration is potential. K_e is highly dynamic and becomes active after a wetting event (rain or irrigation). It decreases as the topsoil dries out. K_e is resonsible for spikes in K_c after wetting events (see figure 28).

In SWAP, actual evapotranspiration (ET_a) is calculated from three quantities for three uniform surfaces:

- ET_{w0}: evapotranspiration rate from a wet canopy, completely covering the soil. Calculated as $ET_{w0} = K_{cf} ET_{ref}$, where K_{cf} is the crop factor.
- ET_{p0}: evapotranspiration rate from a dry canopy, completely covering the soil. Also calculated as $ET_{p0} = K_{cf} ET_{ref}$.
- E_{p0}: evaporation rate from a wet, bare soil. Calculated as $E_{p0} = K_{soil} ET_{ref}$, where K_{soil} is the 'crop' factor for a wet soil.

The crop evapotranspiration is calculated using

$$ET_c = W_{frac} ET_{w0} + (1 - W_{frac}) ET_{p0} \tag{22}$$

with W_{frac} defined as

$$W_{frac} = \frac{P_i}{ET_{w0}}, \quad \text{with} \quad W_{frac} \leqslant 1.0 \tag{23}$$

where P_i (cm h^{-1}) is precipitation intercepted by the canopy. Transpiration and soil evaporation are assumed to be negligible during evaporation of intercepted water; after the intercepted water has evaporated, transpiration and soil evaporation commence again. This is expressed by W_{frac} (-), the fraction of time that the canopy is wet,

calculated as In this study, the vegetative soil cover is used in SWAP rather than LAI. Potential soil evaporation is calculated with

$$E_p = (1 - W_{frac})(1 - SC)K_{soil}ET_{ref} \tag{24}$$

where SC (-) is vegetative soil cover. Subsequently, transpiration is calculated with

$$T_p = (1 - W_{frac})ET_{p0} - E_p \tag{25}$$

Note: greater potential soil evaporation leads to less potential transpiration. If $K_{soil} = K_{crop}$, then equation 25 becomes

$$T_p = SC(1 - W_{frac})ET_{p0} \tag{26}$$

This approximation is the one that has been used to calculate the crop factors.[1]

Crop coefficients from vegetation height and vegetative soil cover

The basal crop coefficient (K_{cb}) normally refers to a crop that is non-stressed and well managed. For natural, non-pristine, or non-typical vegetation FAO-56 introduces a basal crop coefficient that explicitly refers to full vegetative cover. It approximates it as a function of vegetation height and climate as

$$K_{cb,full} = F_r\left(K_{cb,h} + \left[0.04(u_2 - 2) - 0.004(RH_{min} - 45)\right]\left(\frac{h}{3}\right)^{0.3}\right) \tag{27}$$

where $K_{cb,full}$ (-) is the basal crop coefficient of a crop that fully covers the ground, Fr (-) is a resistance correction factor for stomatal control on transpiration, $K_{cb,h}$ (-) is the basal crop coefficient for full cover under subhumid and calm wind conditions ($RH_{min} = 45\%$ and $u_2 = 2$ m s^{-1}), u_2 (m s^{-1}) is the mean wind speed at 2 m height, RH_{min} (%) is the mean value for minimum daily relative humidity, and h is mean maximum vegetation height (m). This crop coefficient is for areas of vegetation that are greater than a few hectares. For areas smaller than a few hectares, crop coefficients may exceed those calculated with equation (27) if the vegetation is higher than its surroundings.

The resistance factor for stomatal control (Fr) is calculated as

$$F_r = \frac{\Delta_v + \gamma(1 + 0.34u_2)}{\Delta_v + \gamma(1 + 0.34u_2\frac{r_l}{100})} \tag{28}$$

1 This is accidental. I used incorrect information from the 2008 SWAP user manual and the simulations had already been performed at the time of discovery. In the 2008 manual, T_p is defined as equation (26), with T_p independent of E_p. The 2009 user manual has the correct equation, (25). Fortunately, it makes almost no difference whether equation (25) or (26) is used: calculated crop factors differ by about one percent.

where Δ_v (kPa °C^{-1}) is the slope of the vapour pressure curve, γ (kPa °C^{-1}) is the psychometric constant, and r_l (s m^{-1}) is the crop mean leaf resistance. This factor corrects for vegetation that exhibits more stomal control on transpiration than what is typical for most crops. F_r is often 1.0 as most crops have a mean leaf resistance equal to the reference crop ($r_l = 100$ s m^{-1}). Since leaf resistance was not measured, values for r_l were taken from Descheemaeker et al. (2011).

The basal crop coefficient for full vegetative cover under humid and calm wind conditions is

$$K_{cb,h} = 1.0 + 0.1h, \quad \text{with} \quad K_{cb,h} \leqslant 1.2 \tag{29}$$

The value of 1.2 is a general upper limit for tall vegetation, fully covering the ground, under conditions of $RH_{min} = 45\%$ and $u_2 = 2$ m s^{-1}.

The basal crop coefficient for natural or non-pristine vegetation is then calculated with

$$K_{cb} = K_{c,min} + K_d(K_{cb,full} - K_{c,min}) \tag{30}$$

where $K_{c,min}$ (-) is the minimum crop coefficient for bare soil in the presence of vegetation ($K_{c,min} \approx 0.0$-0.15), and K_d (-) is a vegetation density dependent coefficient, defined as

$$K_d = \min[1, M_L\ f_{c,eff}, (f_{c,eff})^{\frac{1}{1+h}}] \tag{31}$$

where $f_{c,eff}$ (m^2 m^{-2}) is effective fraction of ground cover or shaded by vegetation near solar noon, and M_L is a multiplier on $f_{c,eff}$ describing the effect of canopy density on shading and on maximum relative evapotranspiration per fraction of ground shaded. In FAO-56 $M_L = 2.0$, which was updated by Allen and Pereira (2009) to a range of $M_L = 1.5$-2.0.

$f_{c,eff}$ is corrected for the angle of the sun. Following FAO-56, it is calculated as

$$f_{c,eff} = \frac{f_c}{\sin(\phi)\sin(\delta) + \cos(\phi)\cos(\delta)} \leqslant 1 \tag{32}$$

where f_c (-) is the fraction of ground covered measured perpendicularly to the earth's surface, ϕ (rad) is latitude, and δ (rad) is solar declination. δ is calculated as

$$\delta = 0.409 \sin(2\pi/365\ J - 1.39) \tag{33}$$

where J (-) is the day of year. To get a single value for the crop factor, the value of $\sin(\phi)\sin(\delta) + \cos(\phi)\cos(\delta)$ was averaged.

Converting FAO-56 crop coefficients to SWAP crop factors

The objective is to convert the crop coefficients estimated with FAO-56 so they can be used as inputs for SWAP. However, SWAP has only two input variables: vegetative soil cover SC and the crop factor K_{cf}.

Since FAO-56 K_{cb} and SWAP K_{cf} are nearly the same,

$$T_p = K_{cf}\ SC\ ET_{ref} \approx K_{cb} ET_{ref} \tag{34}$$

where T_p (mm d^{-1}) is potential transpiration. Dividing by ET_{ref} and substituting K_{cb} in equation (30) gives

$$K_{cf}\ SC \approx K_{c,min} + K_d(K_{cb,full} - K_{c,min}) \tag{35}$$

The vegetative soil cover SC in SWAP and the density coefficient K_d in FAO-56 has similar function, as they both reduce the potential transpiration from a crop completely covering the ground to a crop only partially covering the ground. Since SWAP calculates basal soil evaporation separately, $K_{c,min}$ can be set to 0 so that equation (35) becomes

$$K_{cf}\ SC = K_{cb,full}\ K_d \tag{36}$$

SWAP requires SC for partitioning evapotranspiration between transpiration and evaporation. Therefore, SC has to be retained in SWAP, but K_{cf} can be changed. Correcting for SC gives

$$K_{cf} = \frac{K_{cb,full}\ K_d}{SC} \tag{37}$$

Composite canopies

An issue arises when there are multiple canopies to be simulated in SWAP as SWAP simulates only a single crop canopy, while much of the land on St. Eustatius is covered by grass, herbaceous, and shrub vegetation. However, multiple crops can be represented by a single crop factor (K_{cf}) and a single vegetative soil cover (SC) for SWAP, using methods for intercropping provided in FAO-56.

The upper limit for the crop coefficient is given by

$$K_{c,max} = \max\left[\left(1.2 + (0.04(u_2 - 2) - 0.004(RH_{min} - 45)\right)\left(\frac{h}{3}\right)^{0.3}, (K_{cb} + 0.05)\right] \tag{38}$$

where $K_{c,max}$ (-) is the maximum crop coefficient, and K_{cb} is the basal crop coefficient of the taller crop.

For vegetation where the higher crop extends down to the same height as the top of the shorter crop, a crop coefficient for the field can be calculated with

$$K_{c,field} = \frac{\sum_{j=1}^{N_c} f_j h_j K_{cb\ j}}{\sum_{i=1}^{N_c} f_j h_j} \tag{39}$$

where $K_{c,field}$ (-) is the the crop coefficient for the field, N_c is the number of crops in the field, f_j (-) is the fraction of the field planted with the crop, h_j (m) vegetation height, and $K_{cb\ i}$ (-) the basal crop coefficient of the crop j in question. Finally, SWAP vegetative soil cover SC can then be determined as

$$SC = \sum_{i=1}^{N_c} f_i\ f_{c,eff\ i} \tag{40}$$

Only the shrubland required the use of equations (39) and (40), as it is a combination of two distinct types of vegetation, grass and shrubs. The f_i was found per shrubland landscape unit by analyzing satelite images using the program SamplePoint (Booth et al., 2006). This program was used to place points in a grid on a satellite image. Then, every point is classified (in this case, either into shrub or grass). Fraction f_i for a crop is found by dividing the number of points classified as that crop by the total number of points. 255 points were classified per image, 10 images in total, one per shrubland unit identified in figure 9.

Crop factors for shrubland were calculated by first determing separate crop coefficients K_{cb} and effective ground cover $f_{c,eff}$ for the grass vegetation and the shrub vegetation. These were then combined using equations (39) and (40). Finally, equation (37) was used to calculate the crop factor used in SWAP.

B

APPENDIX B: MORRIS METHOD

The methods used to set up trajectories for the Morris method, which was originally described in Morris (1991), are described below. Methods to select optimize trajectories as suggested by Campolongo et al. (2007) are also described in this appendix. These methods were implemented using the R programming language (R Core Team, 2014).

Let the model output under scrutiny be y (water flow from the bottom of the simulated soil column in our case), and $\mathbf{x}$ the k-dimensional vector of the model factors. $\mathbf{x}^{(l)}$) and $\mathbf{x}^{(l+1)}$, with l in the set $\{1, \ldots, k\}$, are points points sampling the input space, differing in their ith component. Then, the elementary effect $d_i(\mathbf{x}^{(l)})$ for that factor i is

$$d_i(\mathbf{x}^{(l)}) = \frac{y(\mathbf{x}^{(l+1)}) - y(\mathbf{x}^{(l)})}{x_i^{(l+1)} - x_i^{(l)}} \tag{41}$$

See figure 29 for a graphical example.

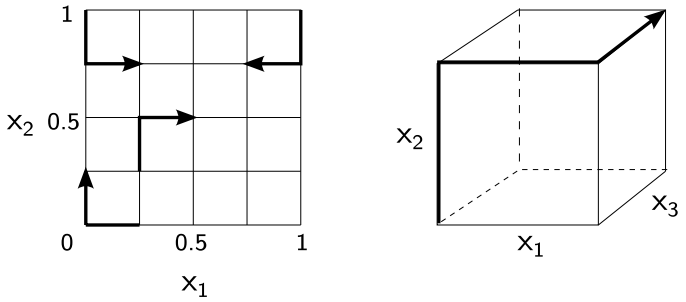

Figure 29: Example Morris experiment trajectories. The left figure depicts r=4 trajectories for k=2 dimensions, for p=5 levels. Every trajectory has k+1=3 points. After the model is run for a trajectory, two elementary effects can be calculated: between the first and second point, and between the second and third point of the trajectory. The right figure shows a trajectory for k=3.

Following Morris (1991), p was chosen even, $\Delta = p/(2(p-1))$, and a number of vectors and matrices are created to obtain random trajectories:

1. Matrix $\mathbf{B}$ is a $(k+1) \times k$ dimensioned strictly lower triangular matrix of 1s.

2. $\mathbf{x}^*$ is a vector containing the factors, for each factor its level randomly selected from the set $\{0, 1/(p-1), 2/(p-1), \ldots, 1-\Delta\}$, each with equal probability. It is the starting point of a trajectory.

3. $\mathbf{D}^*$ is a diagonal matrix in which each diagonal element is either 1 or -1, with probability 0.5 each.

4. $\mathbf{J}_{k+1,k}$ and $\mathbf{J}_{k+1,1}$ are a $(k+1) \times k$ dimensioned matrix and a $(k+1)$ dimensioned column matrix, respectively, both with all elements 1.

5. $\mathbf{P}^*$ is a $k \times k$ dimensioned random permutation matrix, in which each column and each row holds one 1.

Then, we may construct for every trajectory a matrix $\mathbf{B}^*$, in which each row is a point in the trajectory that holds the k number of factor values, as follows

$$\mathbf{B}^* = (\mathbf{J}_{k+1,1}\mathbf{x}^* + (\Delta/2)[(2\mathbf{B} - \mathbf{J}_{k+1,k})\mathbf{D}^* + \mathbf{J}_{k+1,k}])\mathbf{P}^* \tag{42}$$

The superscript * denotes an array thas involves randomness and may differ between trajectories. $(\Delta/2)[(2\mathbf{B} - \mathbf{J}_{k+1,k})\mathbf{D}^* + \mathbf{J}_{k+1,k}$ appoints the factor changes. $\mathbf{P}^*$ is responsible for shuffling the order in which the factors are changed in the trajectory.

For the following example, consider a model with number of parameters $k = 3$, number of levels $p = 4$, and $\Delta = p/(2(p-1)) = 2/3$. Following the five steps, we get:

1. $\mathbf{B} = \begin{pmatrix} 0 & 0 & 0 \\ 1 & 0 & 0 \\ 1 & 1 & 0 \\ 1 & 1 & 1 \end{pmatrix}$

2. $\mathbf{x}^* = \begin{pmatrix} 0 \\ 1/3 \\ 1/3 \end{pmatrix}$

3. $\mathbf{D}^* = \begin{pmatrix} -1 & 0 & 0 \\ 0 & -1 & 0 \\ 0 & 0 & 1 \end{pmatrix}$

4. $\mathbf{J}_{4,3} = \begin{pmatrix} 1 & 1 & 1 \\ 1 & 1 & 1 \\ 1 & 1 & 1 \\ 1 & 1 & 1 \end{pmatrix}$ and $\mathbf{J}_{4,1} = \begin{pmatrix} 1 \\ 1 \\ 1 \\ 1 \end{pmatrix}$

5. $\mathbf{P}^* = \begin{pmatrix} 0 & 1 & 0 \\ 0 & 0 & 1 \\ 1 & 0 & 0 \end{pmatrix}$

Filling in $\mathbf{B}^* = (\mathbf{J}_{k+1,1}\mathbf{x}^* + (\Delta/2)[(2\mathbf{B} - \mathbf{J}_{k+1,k})\mathbf{D}^* + \mathbf{J}_{k+1,k}])\mathbf{P}^*$ gives:

$$\mathbf{J}_{k+1,1}\mathbf{x}^* = \begin{pmatrix} 1 \\ 1 \\ 1 \\ 1 \end{pmatrix} \begin{pmatrix} 0 & 1/3 & 1/3 \end{pmatrix} = \begin{pmatrix} 0 & 1/3 & 1/3 \\ 0 & 1/3 & 1/3 \\ 0 & 1/3 & 1/3 \\ 0 & 1/3 & 1/3 \end{pmatrix}$$

$$2\mathbf{B} - \mathbf{J}_{k+1,k} = 2 \begin{pmatrix} 0 & 0 & 0 \\ 1 & 0 & 0 \\ 1 & 1 & 0 \\ 1 & 1 & 1 \end{pmatrix} - \begin{pmatrix} 1 & 1 & 1 \\ 1 & 1 & 1 \\ 1 & 1 & 1 \\ 1 & 1 & 1 \end{pmatrix} = \begin{pmatrix} -1 & -1 & -1 \\ 1 & -1 & -1 \\ 1 & 1 & -1 \\ 1 & 1 & 1 \end{pmatrix}$$

$$(2\mathbf{B} - \mathbf{J}_{k+1,k})\mathbf{D}^* + \mathbf{J}_{k+1,k} = \begin{pmatrix} -1 & -1 & -1 \\ 1 & -1 & -1 \\ 1 & 1 & -1 \\ 1 & 1 & 1 \end{pmatrix} \begin{pmatrix} 1 & 0 & 0 \\ 0 & -1 & 0 \\ 0 & 0 & 1 \end{pmatrix} = \begin{pmatrix} 1 & 1 & -1 \\ -1 & 1 & -1 \\ -1 & -1 & -1 \\ -1 & -1 & 1 \end{pmatrix}$$

$$(\Delta/2)[(2\mathbf{B} - \mathbf{J}_{k+1,k})\mathbf{D}^* + \mathbf{J}_{k+1,k}] = 1/3 \left[\begin{pmatrix} 1 & 1 & -1 \\ -1 & 1 & -1 \\ -1 & -1 & -1 \\ -1 & -1 & 1 \end{pmatrix} + \begin{pmatrix} 1 & 1 & 1 \\ 1 & 1 & 1 \\ 1 & 1 & 1 \\ 1 & 1 & 1 \end{pmatrix} \right] = \begin{pmatrix} 2/3 & 2/3 & 0 \\ 0 & 2/3 & 0 \\ 0 & 0 & 0 \\ 0 & 0 & 2/3 \end{pmatrix}$$

$$\mathbf{J}_{k+1,1}\mathbf{x}^* + (\Delta/2)[(2\mathbf{B} - \mathbf{J}_{k+1,k})\mathbf{D}^* + \mathbf{J}_{k+1,k}] = \begin{pmatrix} 0 & 1/3 & 1/3 \\ 0 & 1/3 & 1/3 \\ 0 & 1/3 & 1/3 \\ 0 & 1/3 & 1/3 \end{pmatrix} + \begin{pmatrix} 2/3 & 2/3 & 0 \\ 0 & 2/3 & 0 \\ 0 & 0 & 0 \\ 0 & 0 & 2/3 \end{pmatrix} = \begin{pmatrix} 2/3 & 1 & 1/3 \\ 0 & 1 & 1/3 \\ 0 & 1/3 & 1/3 \\ 0 & 1/3 & 1 \end{pmatrix}$$

$$\mathbf{B}^* = (\mathbf{J}_{k+1,1}\mathbf{x}^* + (\Delta/2)[(2\mathbf{B} - \mathbf{J}_{k+1,k})\mathbf{D}^* + \mathbf{J}_{k+1,k}])\mathbf{P}^* = \begin{pmatrix} 2/3 & 1 & 1/3 \\ 0 & 1 & 1/3 \\ 0 & 1/3 & 1/3 \\ 0 & 1/3 & 1 \end{pmatrix} \begin{pmatrix} 0 & 1 & 0 \\ 0 & 0 & 1 \\ 1 & 0 & 0 \end{pmatrix} = \begin{pmatrix} 1/3 & 2/3 & 1 \\ 1/3 & 0 & 1 \\ 1/3 & 0 & 1/3 \\ 1 & 0 & 1/3 \end{pmatrix}$$

So that $x^{(1)} = (1/3, 2/3, 1)$; $x^{(2)} = (1/3, 0, 1)$; $x^{(3)} = (1/3, 0, 1/3)$; $x^{(4)} = (1, 0, 1/3)$. These four points in the input space form a single trajectory.

To get multiple trajectories, we use equation (42) many times, for example r times. With $\mathbf{x}^*$, $\mathbf{D}^*$, and $\mathbf{P}^*$ are randomly generated, we get a set of independent trajectories. For additional information, see Saltelli et al. (2004) or Morris (1991).

To investigate global sensitivity well, the trajectories should cover the entire area of the input space that is being investigated; all trajectories should not be located in the same corner of the input space. (Campolongo et al., 2007) suggest a space filling design. To cover the area of experimentation in the input space well, r trajectories may be selected in such a way that they are maximally scattered across the input space. The distance between the two differing trajectories m and o may be defined as

$$d_{m,o} = \begin{cases} \sum_{v=1}^{k+1} \sum_{w=1}^{k+1} \sqrt{\sum_{z=1}^{k} [x_v^m(z) - x_w^o(z)]^2} & \text{for } m \neq l \\ 0 & \text{otherwise} \end{cases} \tag{43}$$

where $x_v^o(z)$ indicates the zth coordinate of the vth point in the mth Morris trajectory. In brief, the geometric distance is calculated between every point (with k dimensions) in m and every point in o, and the sum of all these distances is calculated.

The best set of trajectories is selected by maximizing the distance among the trajectories. Say we have trajectories m, o, and p. We can calculate the distance among them with

$$D_{m,o,p} = \sqrt{d_{m,o}^2 + d_{m,p}^2 + d_{o,p}^2} \tag{44}$$

Similarly, we can calculate the distance among the trajectories, m, o, and q. If $D_{m,o,q} > D_{m,o,p}$ then $D_{m,o,q}$ will be chosen as the best set of trajectories of the two.

Following the recommendations of Campolongo et al. (2007), $p = 4$, $r = 10$, and a brute force approach was used to determine the optimum set of 10 trajectories. First, 20 trajectories were generated. For all possible couples of trajectories, distance has been calculated with equation (43). Then, all combinations of these 20 trajectories have been evaluated using (44), where the set of 10 trajectories with the maximum amount of distance among them has been chosen to be used in the sensitivity analysis.

Finally, actual SWAP input values for a trajectory are calculated from matrix $\mathbf{B}^*$ with

$$\mathbf{V}^* = (\mathbf{B}^*(\kappa_{upper} - \kappa_{lower}) + \mathbf{K}_{k+1,k})\mathbf{M} \tag{45}$$

where $\mathbf{V}^*$ is a $(k+1) \times k$ matrix with elements that are the SWAP inputs to be used in the trajectory, κ_{upper} and κ_{lower} are the upper and lower bound of experimentation respectively, $\mathbf{K}_{k+1,k}$ is $(k+1) \times k$ with each element κ_{lower}, and $\mathbf{M}$ is a k-dimensional diagonal matrix in which each element is the midpoint (baseline) value of a SWAP

factor. Effectively, every SWAP input baseline value is multiplied by a corresponding value.

Taking the example $\mathbf{B}^*$ of before, and $\kappa_{upper} = 1.15$, $\kappa_{lower} = 0.85$. Taking for the SWAP factors, the crop factor at 1.05, the saturated water content at 0.516 $cm^3\ cm^{-3}$, and saturated conductivity at 78.4 cm d^{-1}. Then, $\mathbf{V}^* = (\mathbf{B}^*(\kappa_{upper} - \kappa_{lower}) + \mathbf{K}_{k+1,k})\mathbf{M} =$

$$\left(\begin{pmatrix} 1/3 & 2/3 & 1 \\ 1/3 & 0 & 1 \\ 1/3 & 0 & 1/3 \\ 1 & 0 & 1/3 \end{pmatrix} 0.30 + \begin{pmatrix} 0.85 & 0.85 & 0.85 \\ 0.85 & 0.85 & 0.85 \\ 0.85 & 0.85 & 0.85 \\ 0.85 & 0.85 & 0.85 \end{pmatrix}\right) \begin{pmatrix} 1.05 & 0 & 0 \\ 0 & 0.516 & 1 \\ 0 & 0 & 78.4 \end{pmatrix}$$

This results in: $\mathbf{V}^* = \begin{pmatrix} 0.9975 & 0.5418 & 90.16 \\ 0.9975 & 0.4386 & 90.16 \\ 0.9975 & 0.4386 & 74.48 \\ 0.12075 & 0.4386 & 74.48 \end{pmatrix}$

The values in this matrix are finally written into the SWAP input files. Going from the first to second row, saturated water content changes from 0.5418 to 0.4386 $cm^3\ cm^{-3}$. Running SWAP for the first row and the second row results in two outcomes, which can be compared to calculate the elementary effect for saturated water content. Similarly, running SWAP for the third row and comparing with the outcomes of the second and the third row allows us to calculate the elementary effect for changing saturated conductivity from 90.16 to 74.48 cm d^{-1}.

For the actual sensitivity analyses, these steps were applied using all the parameters listed in table 3. For the first sensitivity analysis, each trajectory requires 32 simulations (one for each parameter, and one more). Using 10 trajectories, this required 320 simulations ($r \times (k+1)$). For the second sensitivity analysis, this required 350 simulations.